CZECH TECHNICAL
UNIVERSITY
IN PRAGUE

F3

Faculty of Electrical Engineering
Department of Control Engineering

Bachelor's Thesis

Advanced steering concept for overactuated vehicle

Jan Belák

Prague, May 2020

Supervisor: Ing. Tomáš Haniš, Ph.D.
Department of Control Engineering
Faculty of Electrical Engineering of the CTU in Prague

BACHELOR‘S THESIS ASSIGNMENT

I. Personal and study details

Student's name: **Belák Jan** Personal ID number: **474778**

Faculty / Institute: **Faculty of Electrical Engineering**

Department / Institute: **Department of Control Engineering**

Study program: **Cybernetics and Robotics**

II. Bachelor’s thesis details

Bachelor’s thesis title in English:

Advanced steering concept for overactuated vehicle

Bachelor’s thesis title in Czech:

Pokročilé koncepty řízení jízdních platform s redundantním ovládáním

Guidelines:

The goal of this thesis is to investigate 4x4x4 vehicle platform steering concept. The over-actuated platform with all wheels steered needs MIMO control system providing human driver with necessary driving capabilities augmentation. The design of vehicle control laws using independent steering angles for each wheel will be develop based on hierarchical approach using SISO control loops.
The thesis will address following points:
1) Modeling of linear and non-linear twin track vehicle system
2) Review of existing academia/industry solutions with implementation of the most promising strategies
3) Design of control law that uses rear axle to increase vehicle controllability and provide vehicle stability, while driver is operating front axle
4) Full Steer-by-wire system using four independent wheels steering angles
5) Simulation based and sub-scale platform testing of designed algorithms

Bibliography / sources:

[1] Dieter Schramm, Manfred Hiller, Roberto Bardini – Vehicle Dynamics – Duisburg 2014
[2] Hans B. Pacejka - Tire and Vehicle Dynamics – The Netherlands 2012
[3] Franklin, Powell, Emami-Naeini: Feedback Control of Dynamics Systems. Prentice Hall, USA
[4] Robert Bosch GmbH - Bosch automotive handbook - Plochingen, Germany : Robet Bosch GmbH ; Cambridge, Mass. : Bentley Publishers

Name and workplace of bachelor’s thesis supervisor:

Ing. Tomáš Haniš, Ph.D., Department of Control Engineering, FEE

Name and workplace of second bachelor’s thesis supervisor or consultant:

Date of bachelor’s thesis assignment: **28.01.2020** Deadline for bachelor thesis submission: **22.05.2020**

Assignment valid until: **30.09.2021**

Ing. Tomáš Haniš, Ph.D.	prof. Ing. Michael Šebek, DrSc.	prof. Mgr. Petr Páta, Ph.D.
Supervisor’s signature	Head of department’s signature	Dean’s signature

III. Assignment receipt

The student acknowledges that the bachelor’s thesis is an individual work. The student must produce his thesis without the assistance of others, with the exception of provided consultations. Within the bachelor’s thesis, the author must state the names of consultants and include a list of references.

.	
Date of assignment receipt	Student’s signature

Acknowledgement / Declaration

I would like to use this opportunity to thank my supervisor Ing. Tomáš Haniš, Ph.D. for his advice and support during my work on this thesis.

I would also like to thank my family and friends for their support during my studies.

Last but not least, I would also like to thank all teachers for providing me with the theoretical knowledge necessary for the creation of this thesis.

I hereby declare that I have written this thesis independently according to my theoretical and practical knowledge, consultations and found literature. I also declare that I have cited all used sources in the compliance with Methodical Instructions of the ethical principles for writing an academic thesis.

Prague, 19. May 2020

.....

Abstrakt / Abstract

Tato práce představuje několik strategií řízení príčné dynamiky vozidel s možností natáčení všech čtyř kol. Na začátku práce je odvozen dvoustopý model auta, zaměřený na jednoduchou identifikaci parametrů vozidla. Tento model je poté použit pro odvození řídicích algoritmů, představených v této práci. Výhody vozidel s natáčením všech čtyř kol jsou ukázany pomocí algoritmů, řídících zatáčení zadní nápravy. Tento přístup je dále rozšířen na laterální steer-by-wire řídicí systém s možností nezávislého zatáčení všech čtyř kol. Tento přístup umožnuje řidiči odděleně ovládat stacivou rychlost a boční rychlost vozidla. Řízení laterálního úhlu smyku je použito pro zajištění robustní stability a chování systému. Veškeré vyvinuté algoritmy jsou ověřeny a otestovány na verifikační RC platformě.

Klíčová slova: Laterální dynamika vozidla, Řízení zadní nápravy, Steer-by-wire, Laterální úhel skluzu, Dvojstopé vozidlo, Řízení stavů vozidla

This thesis proposes several strategies of lateral dynamics control for four-wheel steering vehicles. Firstly, a mathematical twin-track model is derived with a focus on vehicle identification and setup. This model is then used for the development of control algorithms, presented in this thesis. Secondly, the rear-axle control state of the art strategies are described to show the possibilities of four-wheel steering. This approach is then extended to a lateral steer-by-wire architecture with complete control over all the vehicle's wheels steering angles. This four-wheel-steering design enables the driver to control the vehicle's yaw rate and lateral speed independently. The system uses a wheel's lateral slip angle control to ensure robust stability and response. All the developed algorithms and models are then verified on a sub-scale vehicle platform.

Keywords: Vehicle lateral dynamics, Rear axle steering, Steer-by-wire, Lateral slip angle, Twin-track model, Vehicle states control

Contents /

Tables / Figures

Chapter 1
Introduction

1.1 Motivation

The current automotive industry seems to focus on the development of complex vehicle control systems. The self-driving car's technology is a great example. These designs, however, mostly use front-axle steering architectures. Such driving system lacks the ability to control the vehicle states, such as yaw rate and lateral speed. This limitation can cause difficulties for autonomous driving systems. A solution to this issue seems to be a four-wheel-steering vehicle. Several automotive companies have already used some form of rear-axle steering to increase the vehicle's manoeuvrability and stability.

However, the developed systems are keeping the front axle steering under the driver's control. The main purpose of such system is to modify vehicle dynamics, not to have full control over the vehicle states. A steer-by-wire system is necessary to achieve such regulation. The capabilities of the human driver are enhanced by the proposed steer-by-wire system. The role of the driver is thus revised to a vehicle operator, expressing the desired manoeuvre. The suitable parametrization of lateral manoeuvre might be vehicle yaw rate and lateral velocity. The manoeuvre execution is then carried out by the steering system in the best way possible.

The inspiration for the steer-by-wire system is a fly-by-wire approach, commonly used in the aircraft industry. The implementation of fly-by-wire control significantly increased the safety and the comfort of flight. These systems also enabled the development of a whole new generation of aircrafts, both in civil and military domain, with unprecedented safety and performance capabilities. By implementing these ideas into the automotive industry, similar results can be expected.

1.2 Thesis goals

The following points can summarize the goals of this thesis.

- Derivation of vehicle's mathematical linear and non-linear model. The design is focused on rapid vehicle identification and simple behaviour description.
- Review of existing academia/industry solutions with the implementation of the most promising strategies.
- Design of control law that uses the rear axle to increase the vehicle controllability and stability, while the driver is operating the front axle.
- Full Steer-by-wire system using four independent wheels steering angles and cascade control architecture. Design with a focus on robust stability and response.
- Simulation and a sub-scale platform based testing of designed algorithms. In particular, a comparison between the simulations and real-life system responses.

1.3 Outline

The work is divided into six chapters, including the introduction.

Chapter 2 derives a mathematical description of the twin-track vehicle with extended usage of other sources. The developed non-linear vehicle uses the bond graph design approach for the model derivation. The resulting system is then linearized to enable the usage of linear control theory.

Chapter 3 is a short review of industry usage of rear-axle steering systems. Two systems, using the rear-axle steering control, are implemented as rear-axle steering benchmark.

Chapter 4 presents the lateral drive-by-wire solution of four-wheel steering systems. The system uses three control loops in cascade to ensure robust stability and response. Design, in-line with both robustness conditions is based on a lateral slip control loop that prevents the vehicle from entering unstable situations such as over-steer and under-steer manoeuvres.

Chapter 5 verifies the previously developed algorithms. The testing method uses a sub-scale verification vehicle with implemented controllers.

The future work is proposed in Chapter 6 according to the discovered issues. Chapter 7 summarizes the conclusions from the previous Chapters.

It should be mentioned that all graphs in Chapters 2 to 4 were created with the usage of Matlab and Simulink simulations. The graphs in Chapter 5 were measured with the usage of the sub-scaled verification platform.

Chapter 2
Mathematical description of a twin-track vehicle

2.1 Introduction

The considered system is a four-wheel steering vehicle. A significant number of articles and books have already described the car dynamics [1], [2], [6] and these sources are extensively used as part of the mathematical model derivation. This thesis uses the design methods for SISO LTI systems, and therefore a linearized model also needs to be derived. Model validation and a verification vehicle's identification uses a non-linear vehicle description. After considering all of the above, the goal of this chapter is set to create a simple but still sufficiently accurate description of the vehicle dynamics by adopting the previously developed models. The resulting mathematical model will be verified with respect to the sub-scale demonstrator.

2.2 Vehicle subsystems

An accurate description of the entire car physics can be complicated and is unnecessary in the content of this thesis. Instead, a vehicle can be divided into several essential subsystems. Each subsystem can be modelled independently, with a power interaction used to describe their interconnection. This division is based on the bond graph modelling approach, described in [3, s. 7]. Considering that the car is mostly a mechanical system, the power interaction description can use force and speed interaction between subsystems. As the primary goal of this thesis is to create lateral control laws for vehicle dynamics, the focus of the modelling procedure will be on car dynamics at a constant longitudinal speed. After considering all of the above, the vehicle was divided into the following subsystems.

- Vehicle body
- Suspension
- Wheels
- Powertrain

The interaction between the subsystems is shown in Figure 2.1. The Figure also shows the causality of each interaction. The only exception is the force $F_{z_{ground}}$, describing the ground interaction, based on Pacejka equations. The behaviour of such force is similar to the modulation signal in generalized modulated transformers described in [3].

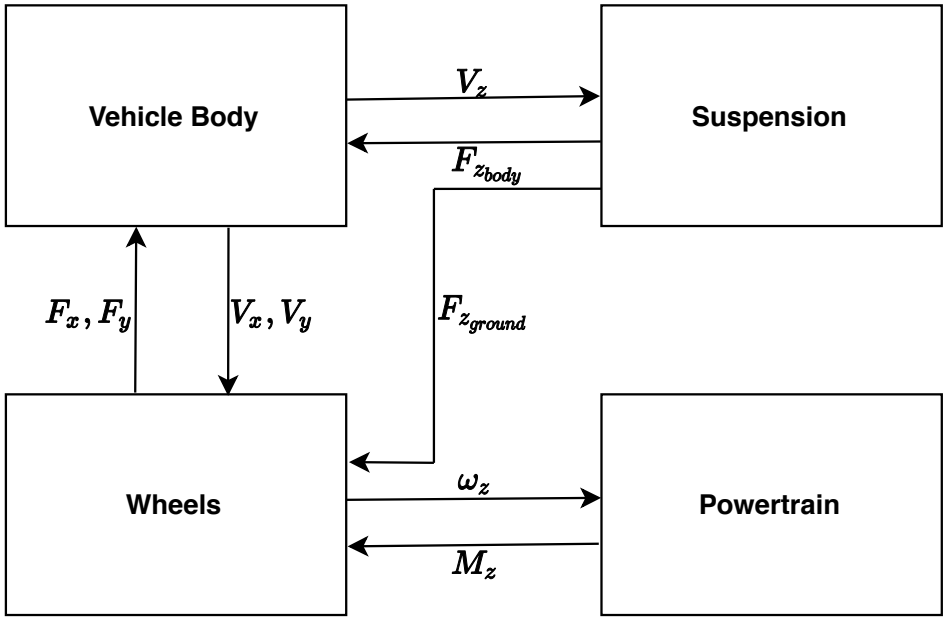

Figure 2.1. Description interaction between the car's subsystems .

2.3 Coordinate systems and variables

The coordinates can be divided according to previously mentioned vehicle subsystems. The upper index is used to distinguish between the coordinate systems. Each system is described by a three-letter upper index. The first determines if the reference system is the vehicle body (b) or wheel (w), the second defines front (f) or rear(r) axle and the third left(l) or right(r) side. The x letters are used for the generalized description of a coordinate system. The vehicle's body coordinate system at the centre of gravity (CoG) does not have the upper index to highlight it as the main system. The essential variables are introduced in the Table 2.1 and the overall vehicle description, inspired by [2, s. 21], is presented in the Figure 2.2. The Figure includes all variables from Table 2.1 as well as variables, described in the following sections.

Term	Symbol	Unit	Definition
Longitudinal speed	v_x	ms^{-1}	Velocity vector x coordinate
Lateral speed	v_y	ms^{-1}	Velocity vector y coordinate
Vertical speed	v_z	ms^{-1}	Velocity vector z coordinate
Yaw angle	β	rad	atan2(v_y,v_x)
Roll angle	ϕ	rad	atan2(v_z,v_y)
Pitch angle	θ	rad	atan2(v_z,v_x)
Wheels turn angle	δ	rad	Angle between x and $x^{X,X}$
Wheels slip angle	α	rad	-atan2($v_y^{X,X}$,$v_x^{X,X}$) + $\delta^{X,X}$
Front length	$C_{x,f}$	m	Length from CoG to vehicle's front
Rear length	$C_{x,r}$	m	Length from CoG to vehicle's rear
Side length	C_y	m	Length from CoG to vehicle's side
Vertical length	C_z	m	Length from CoG to vehicle's top

Table 2.1. Table of essential variables for vehicle description.

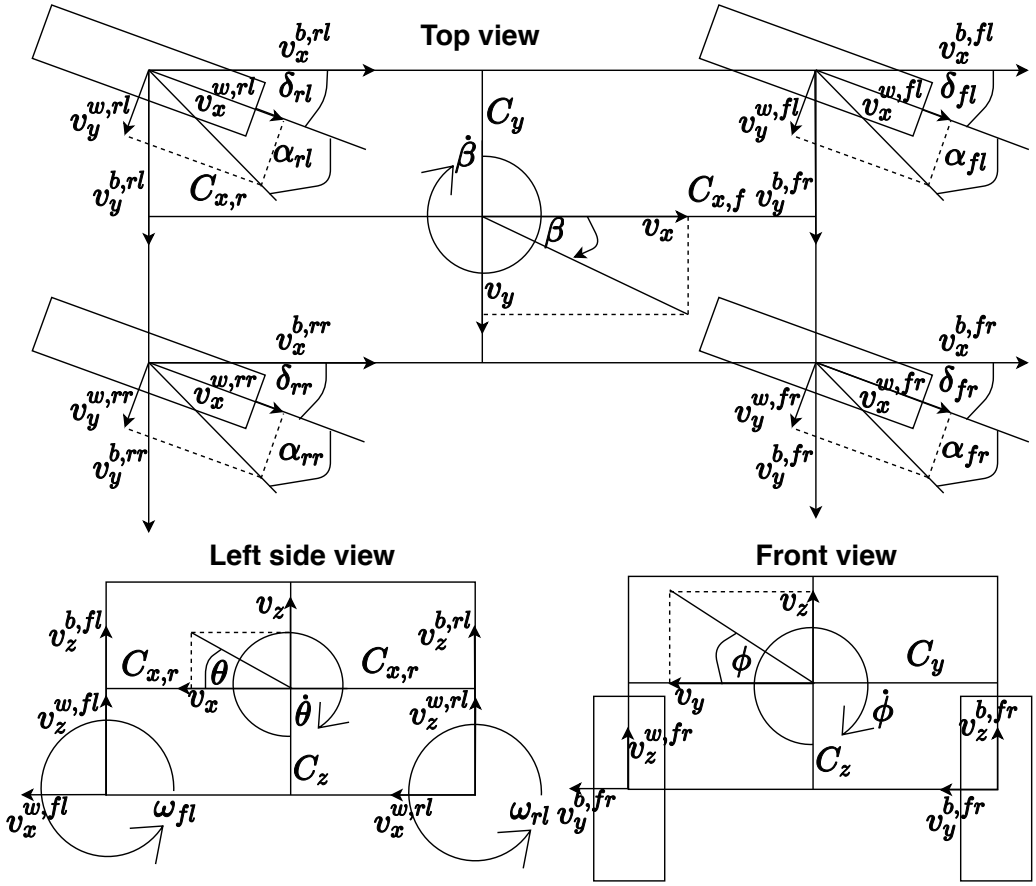

Figure 2.2. Kinematic description of the vehicle.

2.4 Vehicle Body

A common approach for the car body description is to assume that the subsystem is a rigid body of a constant mass. Newton's law of motion and Euler rotation equations for a rigid body of a constant mass have been used for modelling of the subsystem's dynamic behaviour.

2.4.1 Equations of motion

By applying the Newtons and Euler motion laws for a rigid body in 3D space, the following system of equations can be derived.

$$M\dot{\vec{v}} + D\vec{v} = \vec{F} \tag{2.1}$$

$$I_\omega\dot{\vec{\omega}} + \vec{\omega} \times (I\vec{\omega}) = M_{\vec{\omega}} \tag{2.2}$$

where

$$M = I \cdot \begin{pmatrix} m \\ m \\ m \end{pmatrix}, D = I \cdot \begin{pmatrix} d_x \\ d_y \\ d_z \end{pmatrix}, F = \begin{pmatrix} F_x \\ F_y \\ F_z - g \end{pmatrix}, I_\omega = I \cdot \begin{pmatrix} I_\beta \\ I_\phi \\ I_\theta \end{pmatrix}, M_\omega = I \cdot \begin{pmatrix} M_\beta \\ M_\phi \\ M_\theta \end{pmatrix}$$

$m[kg]$ is a mass, $d[-]$ are drag coefficients and $I[kg \cdot m^2]$ are principal moments of inertia of the vehicle body. In the most real-life situations, the pitch and roll rates are low.

Therefore we will not assume the torque, produced by the cross coupling of rotation velocities $\vec{\omega} \times (I\vec{\omega})$. Last unknown constants in the equations are moments of inertia with respect to principal axes of rotation. In this case, we can use Figure 2.2 to derive the equations for moments of inertia. These values I_β, I_ϕ and I_θ for rigid block with given mass is shown in the Equation(2.3).

$$I_\omega = M \cdot \begin{pmatrix} \frac{((C_x f + C_x r) \cdot 0.5)^2 + C_y^2}{12} \\ \frac{C_y^2 + C_z^2}{12} \\ \frac{((C_x f + C_x r) \cdot 0.5)^2 + C_z^2}{12} \end{pmatrix} \tag{2.3}$$

The equations assume evenly distributed mass throughout the block.

2.4.2 External forces

Forces, acting on the vehicle body, can be divided into two groups. The first group are external disturbations, such as the wind. The other subsystems of the car create the second group of forces. This group can be further divided into wheel forces, acting along axes in the longitudinal and lateral direction, and suspension forces, acting in the vertical direction of the car's body. We can assume that the wheels and suspension forces are acting in the same four points of contact (PoC) with the vehicle's body frame. These PoC are assumed to lay at the body's corners. For the modelling procedure, a unified way of forces description needs to be introduced. Each force is described as $F_{component}^{CoordinateSystem}$. The coordinate system description is described in section 2.3. The transformation from the coordinate system at the CoG to PoC can be described as a translation by appropriate vehicle size. The transformation between the vehicle's wheel and body at PoC coordinate systems can be described as rotation by δ.

2.4.3 Vehicle interaction

The description of external forces effect on the subsystem is needed. The generated force in x-direction can be written as $F_x = F_x^{b,fl} + F_x^{b,fr} + F_x^{b,rl} + F_x^{b,rr}$. The same principle applies to the forces F_y and F_z. The principal torques can be determined with the usage of trigonometry. As all the torques can be derived using the same method, only one example is shown. For calculation of the moment M_β, caused by force $F_x^{b,fl}$, description of top view to the body from Figure 2.2 is used. The required force must be projected into the force in direction tangential to yaw rate ,described as F_β, and the force perpendicular to it ,described as $F_\beta^\perp$. The F_β can be calculated as $F_x^{b,fl} \cdot \sin(\alpha) \cdot C_f$, where C_f is distance between the PoC and CoG and α is angle between vectors $C_{x,F}$ and C_f. This angle can be calculated as $\arcsin(C_y/C_f)$. By combining these equations, the relation of M_β with respect to $F_x^{b,fl}$ is $F_x^{b,fl} C_y$. The same process can be used to determine the other moments created by the external forces. All the relations are shown in the Equations (2.4) to (2.8).

$$M_{\beta_f} = C_y \cdot (-F_x^{b,fr} + F_x^{b,fl}) + C_{x,F} \cdot (F_y^{b,fr} + F_y^{b,fl}) \tag{2.4}$$

$$M_{\beta_r} = C_y \cdot (-F_x^{b,rr} + F_x^{b,rl}) - C_{x,R} \cdot (F_y^{b,rr} + F_y^{b,rl}) \tag{2.5}$$

$$M_\beta = M_{\beta_f} + M_{\beta_r} \tag{2.6}$$

$$M_\theta = C_{x,F} \cdot F_z^{b,fx} - C_{x,R} \cdot F_z^{b,rx} + C_z \cdot F_x^{b,fx} + C_z \cdot (F_x^{b,rx}) \tag{2.7}$$

$$M_\phi = C_z \cdot (F_y^{b,xx}) + C_y \cdot (F_z^{b,xr} - F_z^{b,xl}) \tag{2.8}$$

2.4.4 Velocities at the point of contact

The relations between the vehicle's body states and the velocities at the PoC need to be defined for description of power interaction between vehicle subsystems. The same process as for force calculation is used to define the relations (2.9) to (2.16).

$$v_x^{b,xr} = v_x - C_y \cdot \dot{\beta} + C_z \cdot \theta \tag{2.9}$$
$$v_x^{b,xl} = v_x + C_y \cdot \dot{\beta} + C_z \cdot \theta \tag{2.10}$$
$$v_y^{b,fx} = v_y + C_{x,f}\dot{\beta} + C_z \cdot \phi \tag{2.11}$$
$$v_y^{b,r} = v_y - C_{x,r}\dot{\beta} + C_z \cdot \phi \tag{2.12}$$
$$v_z^{b,fr} = v_z + C_z \cdot \theta - C_y \cdot \phi \tag{2.13}$$
$$v_z^{b,fl} = v_z + C_z \cdot \theta + C_y \cdot \phi \tag{2.14}$$
$$v_z^{b,rr} = v_z - C_z \cdot \theta - C_y \cdot \phi \tag{2.15}$$
$$v_z^{b,rl} = v_z - C_z \cdot \theta + C_y \cdot \phi \tag{2.16}$$

The forces and velocities are described in the vehicle's body coordinate system. The transformations to other coordinate systems are defined in section 2.4.2.

2.4.5 Linearization

As the values of roll and pitch rates are typically small, we can omit the coupling parameters while creating only a minor error. With this assumption, the linearized model of the vehicle body can be derived. The motion description is now using linear second-order differential equations. For a control systems design, a state-space description is preferable [4, s. 482-483]. The description, however, requires a system of linear first-order differential equations. Six new coordinates have to be added to convert the motion description into a state-space system. The following list adds six new coordinates to the original description.

- $\Psi = \dot{\beta}$
- $\Theta = \dot{\theta}$
- $\Phi = \dot{\phi}$
- $v_x = \dot{x}$
- $v_y = \dot{y}$
- $v_z = \dot{z}$

Now the state-space system can be derived using the first order differential equations. Unlike the previous description, the new system can be used to track the vehicle position. The system can be described with the usage of A and B matrices [4, s. 482-483], however this form would result in large sparse matrices. To reduce the required space, the system is described with the usage of the first-order differential equations.

$$\dot{\vec{x}} = \vec{v} \tag{2.17}$$
$$M\dot{\vec{v}} = -D\vec{v} + \vec{F} \tag{2.18}$$
$$\dot{\vec{\omega}} = \vec{\Omega} \tag{2.19}$$
$$I_\omega\dot{\vec{\Omega}} = M_\omega \tag{2.20}$$

where M, D, I_ω and M_ω are the matrices, defined at page 5 and $\vec{x} = \begin{pmatrix} x \\ y \\ z \end{pmatrix}$, $\vec{v} = \begin{pmatrix} v_x \\ v_y \\ v_z \end{pmatrix}$, $\vec{\omega} = \begin{pmatrix} \beta \\ \theta \\ \phi \end{pmatrix}$ and $\vec{\Omega} = \begin{pmatrix} \Psi \\ \Theta \\ \Phi \end{pmatrix}$.

2.5 Vehicle suspension

The suspension model is based on [3, s. 94]. The subsystem is divided into four independent parts, one for each wheel. Such configuration is called the quarter-car model, and it is shown in Figure 2.3. For the bond graph description, the m_{body} is replaced by an ideal source of the generalized flow.

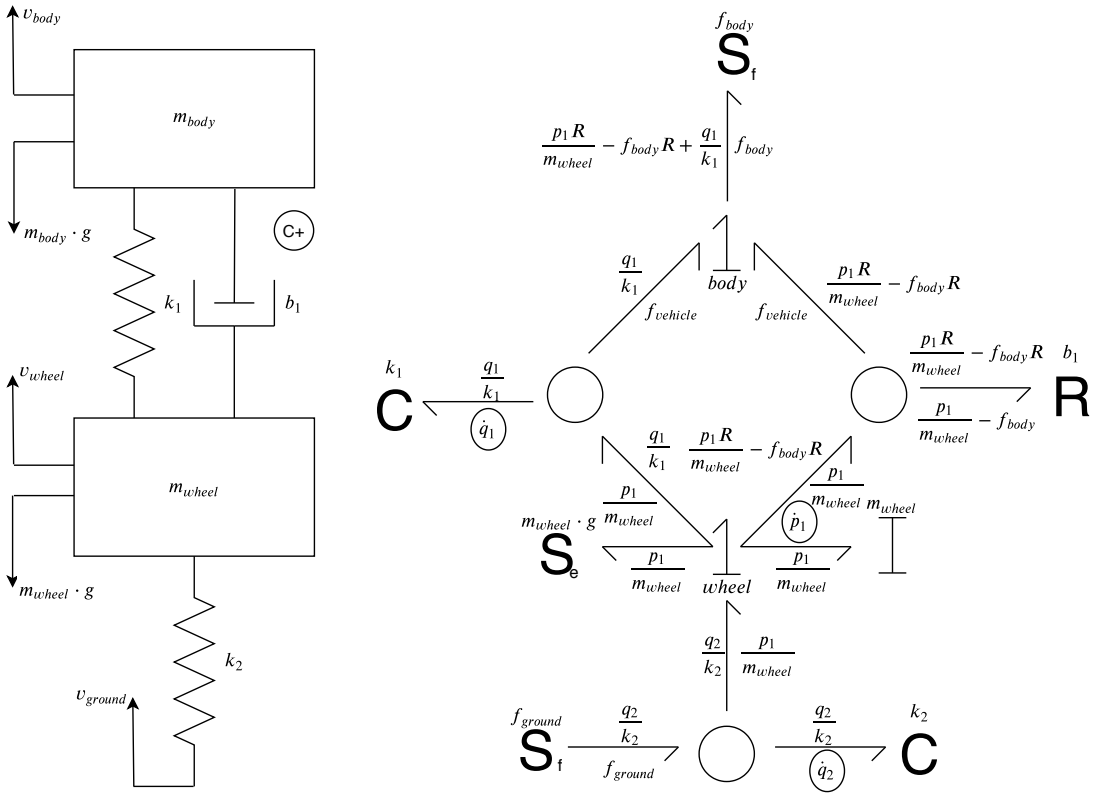

Figure 2.3. The quoter car model based on [3, s. 94]. The Mechanical diagram on the left, the bond graph on the right.

2.5.1 Equations derivation

The bond graph modelling approach was used to derive equations describing the suspension dynamics. The subsystem includes three accumulators of energy and therefore should be described with three independent variables. The chosen variables are compression of the suspension spring q_1, compression of the tire q_2 and vertical position of the wheel p_1. The description of generalized forces and flows is derived according to the process illustrated in [3]. The input velocities from the ground and the vehicle body are modelled as ideal sources of flow $S_f^{f_{body}}$ and $S_f^{f_{ground}}$. The suspension outputs are forces on the body $F_{z,body}$ and the ground $F_{z,ground}$. A state-space description of the system's dynamics is shown in equations (2.21) and (2.22).

$$\begin{pmatrix} \dot{q}_1 \\ \dot{q}_2 \\ \dot{p}_1 \end{pmatrix} = \begin{pmatrix} 0 & 0 & \frac{1}{m_{wheel}} \\ 0 & 0 & \frac{-1}{m_{wheel}} \\ \frac{-1}{k_1} & \frac{1}{k_2} & \frac{-R}{m_{wheel}} \end{pmatrix} \begin{pmatrix} q_1 \\ q_2 \\ p_1 \end{pmatrix} + \begin{pmatrix} -1 & 0 & 0 \\ 0 & 1 & 0 \\ R & 0 & -m_{wheel} \end{pmatrix} \begin{pmatrix} f_c \\ f_g \\ g \end{pmatrix} \tag{2.21}$$

$$\begin{pmatrix} F_{z,body} \\ F_{z,ground} \end{pmatrix} = \begin{pmatrix} \frac{1}{k_1} & 0 & \frac{R}{m_{wheel}} \\ 0 & \frac{1}{k_2} & 0 \end{pmatrix} \begin{pmatrix} q_1 \\ q_2 \\ p_1 \end{pmatrix} + \begin{pmatrix} -R & 0 & 0 \\ 0 & 0 & 0 \end{pmatrix} \begin{pmatrix} f_c \\ f_g \\ g \end{pmatrix} \tag{2.22}$$

2.6 Wheel mathematical model

The mathematical description of the wheel subsystem is based on the Pacejka formula [2]. The Simplified Pacejka magic formula, describing the interaction between tire and ground, has been used.

2.6.1 Wheel parameters

The following parameters must be known for description of the wheel dynamics and traction forces.

- Radius r_{wheel}
- Moment of inertia J_{wheel}
- Pacejka parameters in longitudinal direction B_x, D_x, C_x and E_x
- Pacejka parameters in lateral direction B_y, D_y, C_y and E_y

And the following variables are used for the description of the wheel dynamics.

- Wheel's rotational velocity ω
- Steering angle δ
- Torque, generated by the engine and brakes τ_{EN},τ_{BK}

2.6.2 Wheel dynamics

The wheel is assumed to be a rigid cylinder with a single degree of freedom, represented by the angular velocity around its y-axis. The motion description was implemented according to [2, s. 466-467] , where the torque M_y was added. [2, s. 469]. This definition of M_y is based on statistics and represents the wheel rolling resistance. The final equation can be written as (2.23).

$$\dot{\omega} = \frac{\tau_{EN} - |\tau_{BK}| \cdot sign(\omega) - R_{wheel} \cdot F_x - M_y}{J_{wheel}} \tag{2.23}$$

2.6.3 Coordinates transformation

The Pacejka magic formula uses the vehicle body speed to calculate the forces created by the wheel. However, the body speed needs to be transformed into the wheel's coordinate system and the forces, generated by the wheel, need to be transformed into the vehicle's coordinate system. For the transformation from the wheel's into body's coordinates, the rotation matrix (2.24) is used. As this transformation is invertible, its inversion can be used to transform the coordinates from the body to the wheel coordinate system.

$$R(\delta) = \begin{pmatrix} \cos\delta & \sin\delta \\ -\sin\delta & \cos\delta \end{pmatrix} \tag{2.24}$$

2.6.4 Slip variables

The Pacejka model is using two types of a wheel slip. They are the longitudinal slip ratio and the lateral slip angle. Each variable is referenced to the wheel's coordinate system. The calculation of both values is ill-conditioned at low speeds.

$$\lambda_{xx} = \frac{r_{wheel} \cdot \omega - v_x^{w,xx}}{v_x^{w,xx}} \tag{2.25}$$

$$\alpha_{xx} = -\arctan\frac{v_y^{w,xx}}{v_x^{w,xx}} \tag{2.26}$$

2.6.5 Traction forces

The forces, generated by the wheel are described in [2]. All variables are referenced to the wheel coordinate system. The rotation matrix (2.24) is used for the coordinate transformation. The wheel longitudinal and lateral forces equations are (2.27) and (2.28).

$$F_x^{w,xx} = F_z \cdot D_x \cdot \sin(C_x \cdot \arctan(B_x \cdot \lambda - E_x(B_x \cdot \lambda - \arctan(B_x \cdot \lambda)))) \quad (2.27)$$

$$F_y^{w,xx} = F_z \cdot D_y \cdot \sin(C_y \cdot \arctan(B_y \cdot \alpha - E_y(B_y \cdot \alpha - \arctan(B_y \cdot \alpha)))) \quad (2.28)$$

2.6.6 Traction ellipse

The overall force, generated by the tire, is limited by a traction ellipse [6]. As the equations (2.27) and (2.28) do not assume this limitation, an implementation of traction ellipse according to [6] has been used. The issue connected with this method is that it only saturates the forces according to the traction ellipse shape. Such saturation does not accurately describe the physics behind this phenomenon. This thesis is, however, focused on dynamics and control with small slip ratio and therefore the error is not significant.

2.7 Powertrain

The powertrain subsystem models the dynamics from the driver input to the torque on each wheel. It can be simplified into the engine and the differential. The differential distributes the torque from the engine to the wheels. An assumption of an independent engine at each wheel is used instead of the differential.

2.7.1 Engine

The goal of this modelling approach is to create an accurate model of a vehicle, that can be used for the lateral control systems design and testing. Therefore, an elaborate description of a vehicle engine is not necessary. The creation of such a subsystem description might also create an overall stiff system, which would significantly reduce the vehicle's model capability of a real-time simulations. Due to that, the engine is simplified into a first-order system.

2.8 Linearized dynamics description

The non-linear vehicle model is not suitable for a linear controller design. Therefore, the linearized description of the vehicle is needed. However, the complete linearized vehicle description is not necessary for the controller design. Therefore key smaller subsystems, suitable for linearization process, were selected and a linear model was derived for the purpose of control law development.

- α to yaw rate dynamics
- α to lateral speed dynamics
- δ to α dynamics

As this thesis is focused on lateral dynamics, longitudinal slip ratio is considered to be zero and the vehicle speed constant.

2.8.1 Operation point definition

The operation point is defined by the following values.

- yaw rate φ^{eq}
- longitudinal speed v_x^{eq}
- lateral speed v_y^{eq}
- lateral slip angle α^{eq}

From these values, wheels steering angles can be calculated. By assuming the pitch and roll to be constant, equations (2.9) to (2.16) can be used to calculate the v_x and v_y on each wheel in the vehicle body coordinate system. The lateral slip angle (2.26) can be rewritten with the usage of speed vectors in the body coordinate system.

$$\alpha = \delta - \arctan\frac{v_y^b}{v_x^b} \tag{2.29}$$

2.8.2 Traction forces linearization

The equations (2.27) and (2.28) need to be linearized in order to describe the linear vehicle behaviour. There are several different approaches to linearize these relations [7]. In this thesis, a single gain G_α, G_λ description is implemented. The gain is calculated as partial derivation of equations (2.27) and (2.27) by λ and α respectively. The resulting linear relation is tangent to the original curve. In the following relations, linearization of (2.28) at $\alpha^{eq} = 0$ is mostly used.

The forces $F_x^{w,xx}$ (2.27) and $F_y^{w,xx}$ (2.28) are still referenced to the wheel's coordinate system. The rotation matrix is used to transform these relations into the vehicle body coordinate system.

$$F_x^{b,xx} = \cos\delta F_x^{w,xx} + \sin\delta F_y^{w,xx} \tag{2.30}$$
$$F_y^{b,xx} = -\sin\delta F_x^{w,xx} + \cos\delta F_y^{w,xx} \tag{2.31}$$

By setting the δ equal to δ_0, calculated in(2.29), and to be constant, the linearized transfer from λ and α to F_x^{body} and F_y^{body} is calculated in the Equations (2.32) and (2.33).

$$F_x^{b,xx} = F_{x,0}^{b,xx} + \cos\delta_0 G_\lambda d\lambda + \sin\delta_0 G_\alpha d\alpha \tag{2.32}$$
$$F_y^{b,xx} = F_{y,0}^{b,xx} - \sin\delta_0 G_\lambda d\lambda + \cos\delta_0 G_\alpha d\alpha \tag{2.33}$$

2.8.3 Transfer function from α to yaw rate

The transfer function from a particular wheel's lateral slip angle to the vehicle's yaw rate signal will be introduced in this section. The linearized equation of motion of the yaw rate can be derived from (2.19) and (2.20). The torque M_β, described by equations (2.4) to (2.6), includes traction forces in the x and y-axis of the vehicle body coordinate system. The linearized relation of traction forces in the vehicle body coordinate system is derived in (2.32) and (2.33). By combining these equations, the resulting linear relation for M_β was found to be (2.34) and (2.35). The description assumes zero longitudinal slip ratio at the wheels.

$$M_{\beta_f}^\alpha = \sin(\delta_0)\cdot G_{yf}^{wheel}\cdot Cy\cdot(-\alpha_{fr}+\alpha_{fl}) + \cos(\delta_0)\cdot G_{y,f}^{wheel}\cdot C_{xf}\cdot(\alpha_{fr}+\alpha_{fl}) \tag{2.34}$$
$$M_{\beta_r}^\alpha = \sin(\delta_0)\cdot G_{yr}^{wheel}\cdot Cy\cdot(-\alpha_{rr}+\alpha_{rl}) - \cos(\delta_0)\cdot G_{y,r}^{wheel}\cdot C_{xr}\cdot(\alpha_{rr}+\alpha_{rl}) \tag{2.35}$$
$$M_\beta^\alpha = M_{\beta_f}^\alpha + M_{\beta_r}^\alpha \tag{2.36}$$

The overall linear dynamics equation can be derived by combining the linear torque and motion equations. The resulting yaw rate linearized dynamics can be transformed from state-space description (2.19) and (2.20) into a transfer function using the equation $H(s) = C \cdot (Is - A)^{-1} \cdot B + D$. The resulting transfer function is shown in equation (2.37), where G_{yaw} is $\frac{M_\beta^\alpha}{J_{yaw}}$.

$$tf_{yaw} = \frac{G_{Yaw}}{s} \tag{2.37}$$

Two typical driving situations are used to compare the linear and non-linear systems. The first response, shown in Figure 2.4 on the left, simulates line change situation using three sequential step responses of α_F with car configuration of $v_x^{eq} = 35m \cdot s^{-1}$, $v_y^{eq} = 5m \cdot s^{-1}$ and $\Psi^{eq} = 0\ rad \cdot s^{-1}$. The second response, shown in Figure 2.4 on the left, simulates α_F impulse response with car configuration $v_x^{eq} = 15m \cdot s^{-1}$, $v_y^{eq} = 0m \cdot s^{-1}$ and $\Psi^{eq} = 1rad \cdot s^{-1}$. This situation simulates driving out of a sharp turn in a city. A simple control system is used to ensure each wheel's required lateral slip angle on the non-linear model. The result is shown in the Figure 2.4. The linearized system has an almost identical response on change of α, but the non-linear system is slowly changing yaw rate due to deviation from the operating point.

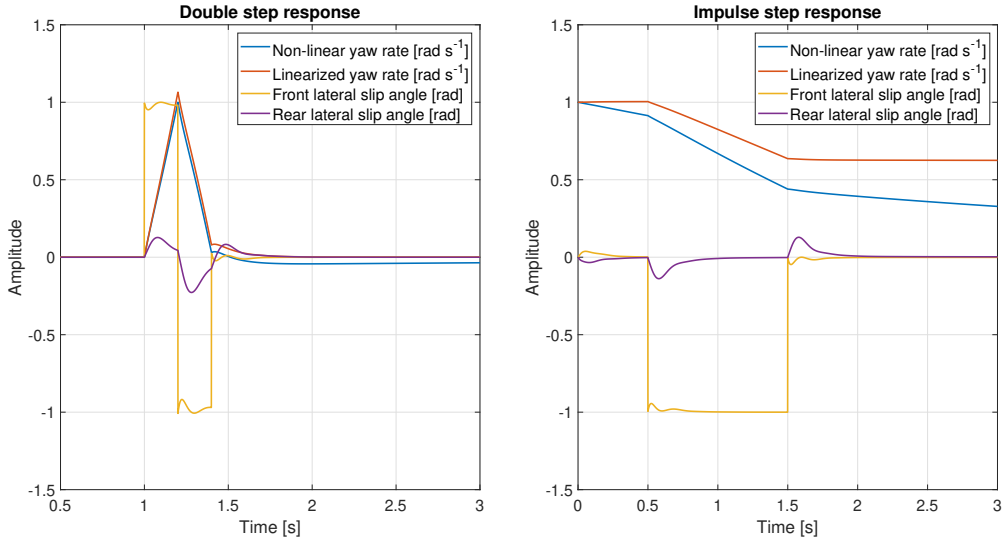

Figure 2.4. Comparison between the linearized and non-linear yaw rate dynamic response with a common lateral slip angle as an input

2.8.4 Transfer function from α to lateral speed

The transfer function from a particular wheel's lateral slip angle to the vehicle's lateral speed signal will be introduced in this section. The linear equations of motion for the vehicle's lateral velocity are shown in (2.17) and (2.18). The lateral speed is only dependent on the traction force in the lateral direction (2.33). The resulting transfer function can be described with a transfer function (2.38), where G_Y is $\frac{F_y^{body}}{m}$. Once the air drag is assumed, the resulting system does not have the astatic behaviour. Nevertheless, the effect of air resistance in the lateral direction can be neglected as the lateral velocity is typically small and thus the system can be assumed to be an integrator with a gain $\frac{F_y^{body}}{m}$. The system was compared to the non-linear model in the same situations, described in section 2.8.3. The results are shown in the Figure 2.5.

$$tf_{yaw} = \frac{G_Y}{s + d_y} \tag{2.38}$$

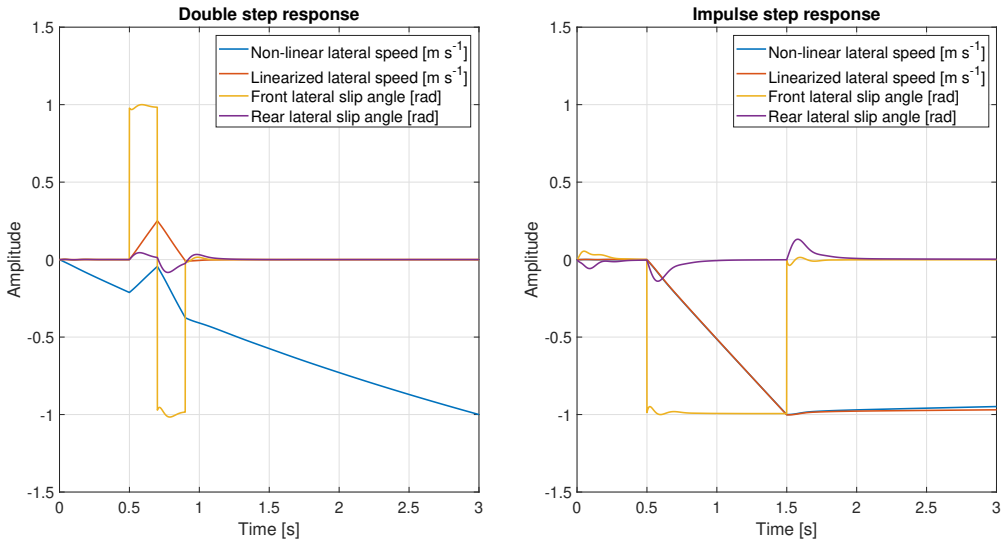

Figure 2.5. Comparison between the linearized and non-linear lateral speed dynamic response with common lateral slip angle as an input

2.8.5 Transfer function from δ to α

The transfer function from particular wheel's steering angle to its lateral slip angle will be introduced in this section. The equation (2.26) and (2.29) are used for the linearization process. The partial derivation of (2.29) with respect to δ describes the isolated dependency of α on δ. This derivation is equal to one. The equation (2.26) describes the dependency of α on $v_x^{w,xx}$,$v_y^{w,xx}$. To determine the effect of α on $v_x^{b,xx}$, $v_y^{b,xx}$, a rotation matrix (2.24) is used. The resulting equation is (2.39).

$$\alpha^{xx} = -\arctan\frac{\cos(\delta^{xx})v_y^{b,xx} - \sin(\delta^{xx}) \cdot v_x^{b,xx}}{\cos(\delta^{xx}) \cdot v_x^{b,xx} + \sin(\delta^{xx})v_y^{b,xx}} \tag{2.39}$$

The partial of equation (2.39) with respect to $v_x^{b,xx}$ and $v_y^{b,xx}$ is used to find linearized dependency of α on velocities in the vehicle body coordinate system. The overall increment of $d\alpha$ is shown in equation (2.40).

$$d\alpha = v_x^{eq}/(v_x^{eq^2} + v_y^{eq^2})dv_y^{b,xx} + v_y^{eq}/(v_x^{eq^2} + v_y^{eq^2})dv_x^{b,xx} + d\delta^{xx} \tag{2.40}$$

The values $dv_y^{b,xx}$ and $dv_x^{b,xx}$ are velocities at the points of contact (PoC) in the vehicle body's coordinate system. By considering the effect of the suspension on the vehicle, we can assume the effect of roll and pitch rate to be insignificant on the resulting values. Then the $v_y^{b,xx}$ is dependent only on the lateral speed and the yaw rate. The $v_x^{b,xx}$ is dependent only on the longitudinal speed and the yaw rate. Linearization of these dynamics is derived in the previous sections 2.8.3 and 2.8.4. The resulted linearized system should only depend on δ, as dλ is considered to be zero. Each wheel must be

designed according to the relevant equation from page 7. The linearized description of the yaw rate and the lateral speed is dependent on all lateral slip angles. Therefore these vehicle states are used to describe the cross-coupling relation between individual wheels. The resulting dynamics is shown in Figure 2.6.

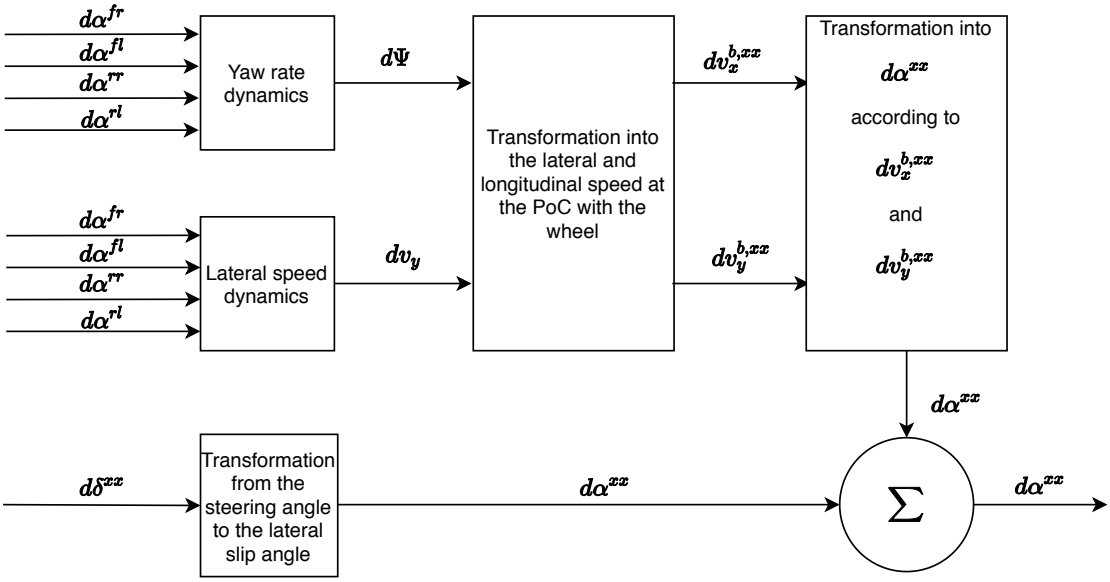

Figure 2.6. Description of linearized δ^{xx} to $d\alpha^{xx}$ dynamics with effect of each $d\alpha$ on the resulting value of $d\alpha^{xx}$

The described system is still not suited for a controller design. The problem is the effect of computed $d\alpha$ on itself. The knowledge of these dynamics independently on other lateral slip ratios would allow designing a feed-forward controller for $d\delta$ to $d\alpha$ control. Vehicle body physics can be divided into the interaction with the current wheel and with other wheels separately to describe the dynamics. The decoupled system is presented in Figure 2.7. The system has an identical response to the description in Figure 2.6. The decoupled system is more suited for controller design. By calculating the closed-loop system, shown in Figure 2.7, the transfer function from δ to α can be determined. The disturbance is also accurately described.

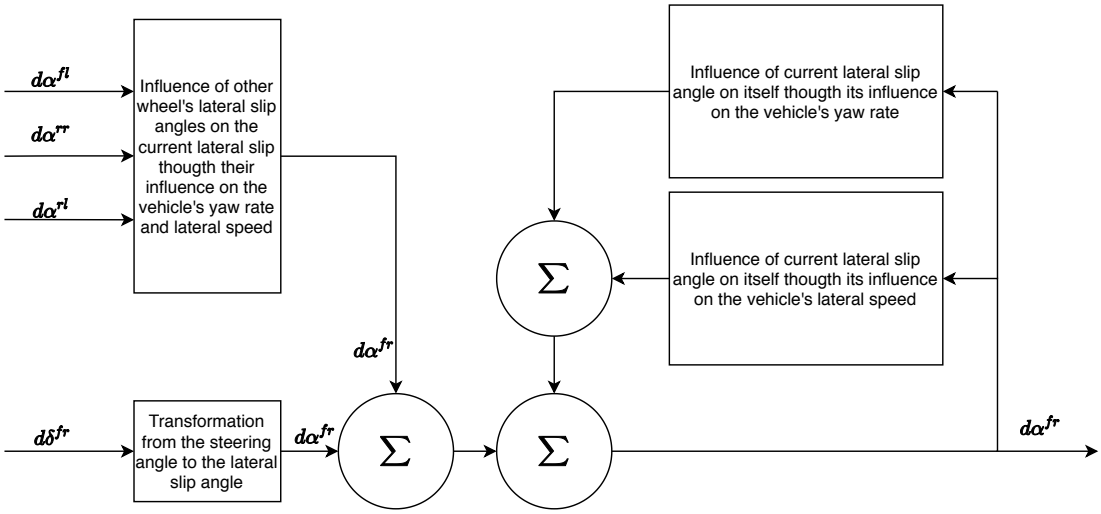

Figure 2.7. Description of decoupled δ^{xx} to $d\alpha^{xx}$ dynamics with effect of other $d\alpha$ on the resulting value of $d\alpha^{xx}$

The same scenarios as in previous chapters were used for testing the linearized α dynamics system. However, δ step response is used as input instead of α. The resulting response for the front right wheel is shown in Figure 2.8.

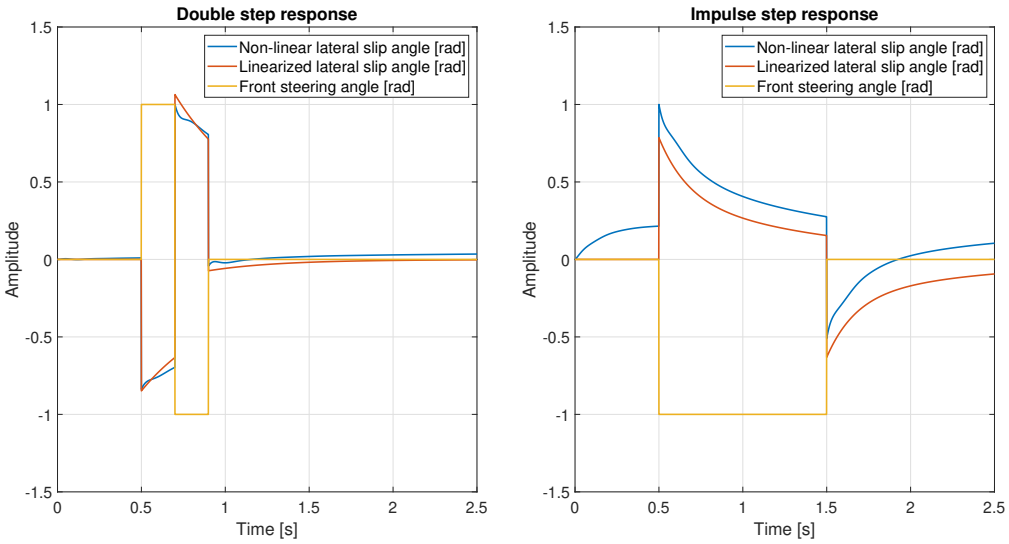

Figure 2.8. Comparison between the linearized and non-linear lateral slip angle dynamic response with common steering angle as an input

2.9 Summary

The resulting mathematical model, derived in this section, allows a simple identification and a reasonably accurate description of the vehicle dynamics. Only basic vehicle parameters are required to set up the model to reflect a vehicle dynamics. This feature allows rapid development of control systems. The drawback of this approach is its relative inaccuracy when compared with more complex models. Therefore, any control systems should be developed with an emphasis on robust stability and response. The linear systems, derived from non-linear vehicle model, can be used for lateral dynamics description and for SISO LTI control law development. As this thesis is focused on the lateral vehicle dynamics, only linear description for the lateral speed, the yaw rate and the lateral slip angle was developed.

Chapter 3
Rear axle steering systems

3.1 Introduction

The transition from the direct front-wheel control to complete four-wheel steering control (4WSC) system is challenging. In this chapter, the selected industrial implementations are presented. The researched industry solutions mostly use rear-axle steering systems (RAS). Therefore, two control systems are proposed to demonstrate the possibilities of RAS systems. The first system, inspired by Audi's four-wheel steering system, uses a feed-forward controller to turn the rear axle according to the vehicle's speed and steering wheel's angle. The second system, inspired by the aerospace industry, uses rear-axle steering to dampen the vehicle's yaw rate and lateral speed. This leads to an increase in the vehicle's stability and manoeuvrability.

3.2 State of the art

The current industry's solutions for 4WSC system can be divided into two approaches. The first is a kinematic control system, implemented on the most four-wheel steering concept vehicles [10],[11]. The second is dependent rear-axle steering system, implemented for example, by Audi and Porsche [12] and [13].

3.2.1 Kinematic steering

Several companies have created concept vehicles with various 4WS systems [10],[11]. All these designs seem to be able to travel only at low speeds. This observation points to the kinematic control design [8],[9]. Such systems do not consider traction forces, slip ratios and other dynamics, necessary to describe the vehicle travelling in high velocities. Therefore these designs seem to be unable to achieve standard vehicle travelling speed. A complete 4WSC system, capable of reaching such a speed, was not found.

An example of such system can be Curiosity Mars rover. The rover has six wheels, from which four are steerable. The system allows the rover to make sharp turns as well as turning in a place. As the rover is a slowly moving vehicle, the system most likely uses kinematic control.

3.2.2 Rear-axle steering system

A dependent RAS system can be used instead of the kinematic steering to allow travelling at a higher speed. This design has control over the rear axle steering angle. However, it keeps the direct control over the front axle in the hands of the driver. The current industry seems to implement mostly dependent RAS systems instead of the complete 4WSC. An example of such design in the industry can be Audi's model Q7 or Porsche 911 Carrera.

According to available information [12] and [13], these systems use feed-forward controller architecture that uses a steering wheel angle to turn the rear wheels. Therefore the driver directly controls the front and indirectly the rear wheels steering angle.

At lower speeds (below 50 km/h), the rear axle turns in the opposite direction and therefore increases the vehicle's agility. In higher speeds (above 80 km/h) the system turns the rear wheels in the same direction as the front axle. The resulting vehicle is more stable then front axle steering design. The system saturates rear axle turn angle to five degrees maximum to prevent unexpected behaviour.

Overall, the system intends to change the vehicle's behaviour without limiting the driver's control over the system. As the controller is dependent on the driver's input, it does not seem to be able to change the wheels turn angle independently. Therefore, systems for slip control are still dependent on torque vectoring systems. The benefit of this design is the lack of complex control systems and sensors. Only the steering wheel turn angle needs to be measured.

3.3 Rear-axle feed forward control law

As part of this Thesis, a feed-forward(FF) rear-wheel controller, inspired by the system from Audi, was developed. The driver has full control over the front wheels steering angle. Feed-forward system proportionally turns the rear wheels according to steering wheel's turn angle. For an increase of the agility at lower speeds, a negative feed-forward gain is used. For an increase of the stability at higher speeds, a positive gain is applied. This relation can be derived from M_β described in (2.34),(2.35) and (2.36). The steering angle gain value is non-linearly dependent on the vehicle speed and is derived in the following text. The overall design is shown in Figure 3.1.

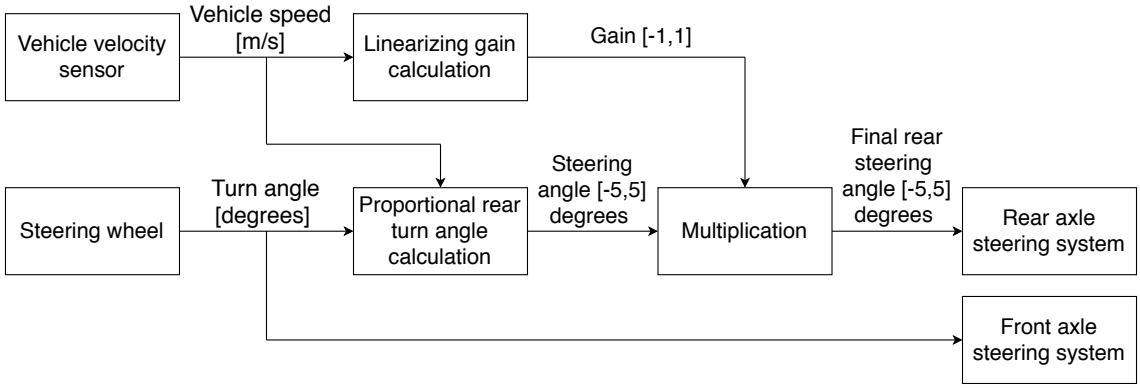

Figure 3.1. Comparison between the linearized and non-linear yaw rate dynamic response

In the case of positive FF gain, the overall M_{beta} can be calculated as $d\alpha_F \cdot C_{xf} - d\alpha_R \cdot C_{xr}$. If the FF system turns the rear wheels too much, the overall torque can have the opposite direction than the driver's initial intention and the system would lose stability. Certain limitation of the rear axle turn ratio is needed. The limit was set according to Audi's system to five degrees maximum. The negative FF system uses the same limitation.

The actual gain value is dependent on the maximal turning angle at a given speed. The value can be determined from an experiment by setting the rear angle to maximal negative angle or maximal positive angle. The vehicle's velocity must be constant. Then the front axle turn angle can be increased by a ramp with a small slope. Maximal turn angle with lateral slip smaller than five degrees can be found using this experiment. The found value is used to calculate the proportional turn angle. The resulting dependency of maximal turn angle on speed is presented in Figure 3.2. According to found dependency, non-linear gain transfer from negative to positive gain is implemented. The used transfer is shown in the same Figure 3.2. The gain changes highly non-linear dependency of the maximal steering angle on the vehicle speed into a linear approximation up to $35m \cdot s^{-1}$. This design improves the controllability of the system from the driver's point of view. The resulting vehicle is significantly more stable and predictable when changing speed.

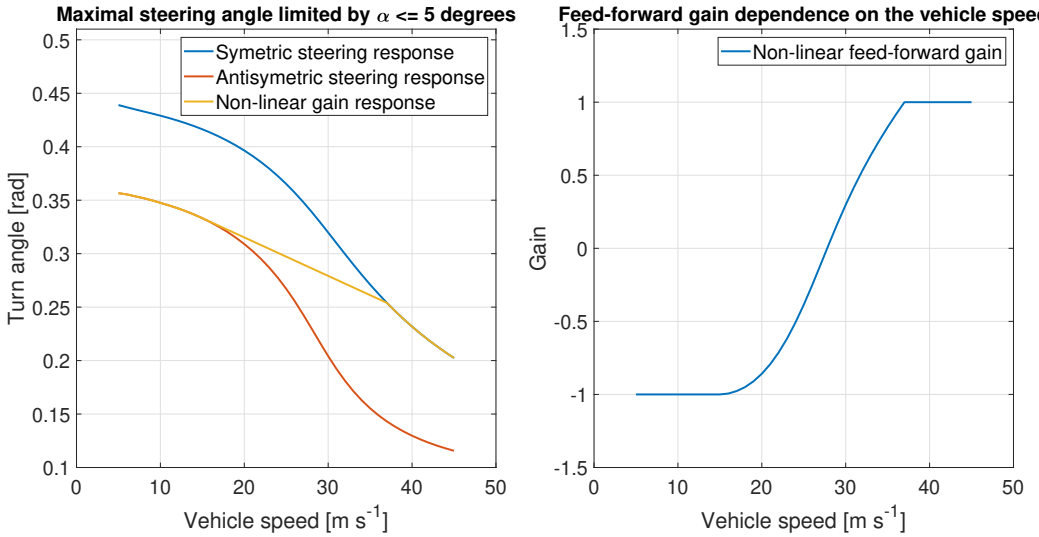

Figure 3.2. Comparison between the linearized and non-linear yaw rate dynamic response

3.4 Rear-axle feedback control law

The previously described algorithms are unable to change the vehicle's behaviour without the driver's input. An independent RAS system is proposed as a transition from a system with driver's full control over the steering to an entirely independent controller. The main idea is to keep the front axle turn angle under the driver's control and use the rear axle for vehicle dynamics shaping. The approach is loosely based on roll, pitch and yaw dumpers, used in the aircraft industry. Such system is supposed to limit the influence of higher frequencies on a system without significantly changing the response of the driver's input.

3.4.1 Controller design

The controller is using a feedback loop to dampen the measured vehicle states to zero. The chosen values are the car's yaw rate and lateral speed. Both values are also directly controlled by the driver, who is steering the front wheels. In order to reduce the controller's influence on the driver's input, a washout filter is used. It is a high-pass filter with zero static gain [14]. By using the filter in the feedback loop, higher frequencies are damped without significantly effecting the controlled state's steady-state value. As

the system is only meant to dampen higher frequencies, a simple gain controller can be used. The overall Washout filter frequency and step responses are shown in Figure 3.4. The system has a time constant of 0.4 seconds. The overall system design is shown in Figure 3.3.

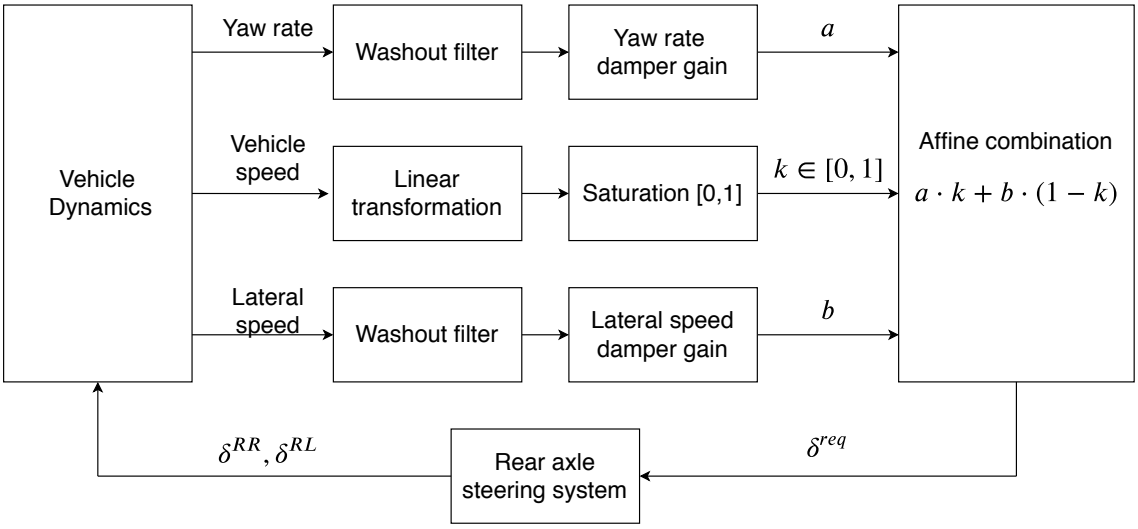

Figure 3.3. Design of a independent rear axle steering controller

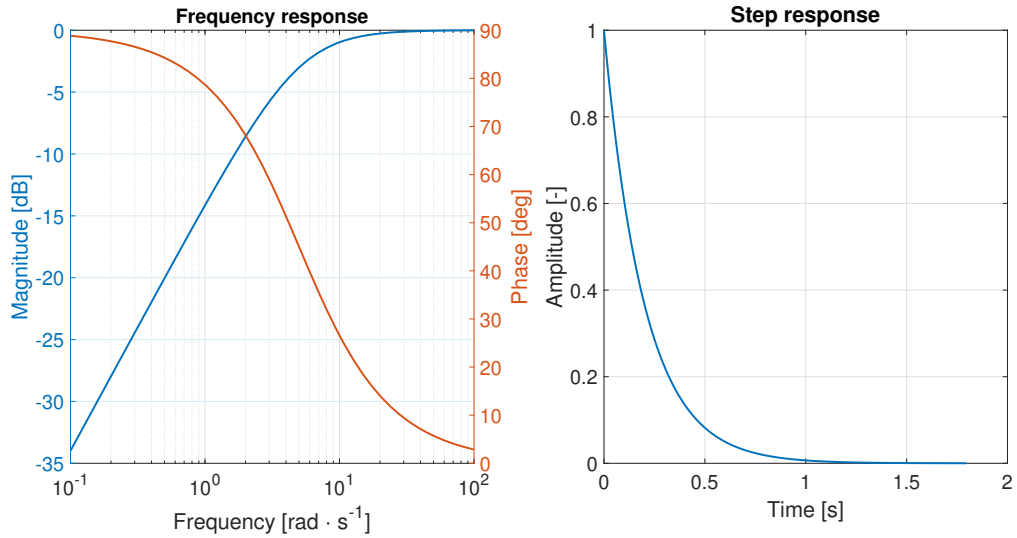

Figure 3.4. Bode plot [left] and step response [right] of a first-order washout filter

The essential vehicle states for damping algorithms are yaw rate and lateral speed. For high velocities, fast changes in yaw rate can lead to the vehicle being unstable. For lower velocities, damping of lateral speed increases the manoeuvrability of the car. Therefore, the combination of yaw rate and lateral speed damper promises to increase the controllability of the system. For the design of the damper, a simple proportional controller can be used. Such system is robust and allows a significant change of the damping strength without losing the system stability. Root Locus algorithm may be used to find gain value for each controller. Linearized transfer function from δ to yaw rate or lateral speed is derived from linearized systems, described in Section 2.8.

Root locus method with usage of a linearized vehicle model was used for the controller derivation. For yaw rate dumper design, the vehicle transfer function was linearized

at $v_x^{eq} = 35m \cdot s^{-1}$, $v_y^{eq} = 0$ $\Psi^{eq} = 0$. For lateral speed damper, the linearization at $v_x^{eq} = 15m \cdot s^{-1}$, $v_y^{eq} = 0$ $\Psi^{eq} = 0$ was used. For both cases, the resulting poles can be set on the real axis. The resulting response is, therefore, without oscillations. As the gain can be set within a relatively large range of values, the damping strength can be changed according to the driver's input without risk of instability or occurrence of oscillations. This feature can be used to change vehicle stability manually in slippery ground conditions or to increase agility in optimal conditions.

3.4.2 Lateral dampers effect

The step response is used to show the behaviour of the designed dampers. The front wheels are turned by one degree at constant vehicle speed. The lateral speed damper's response is shown in Figure 3.6. The lateral speed changes slower with the damper than with a fixed rear axle system. The other effect of the damper is an increase of yaw rate at the beginning of the manoeuvre. For the driver, the result is a more agile and faster-turning vehicle. The response is ideal for slow-speed situations.

The yaw rate damper's response is shown in Figure 3.5. It can be seen that the damper reduces the change of yaw rate and instead increases the vehicle's lateral speed. In high-speed situations, fast change of yaw rate can lead to unstable vehicle behaviour. Avoiding unexpected obstacle can be considered as an example. In such a situation, yaw rate damper increases the stability of the vehicle and enables sharper and faster avoidance of the obstacle. This is due to the initial increase in the lateral speed of the vehicle.

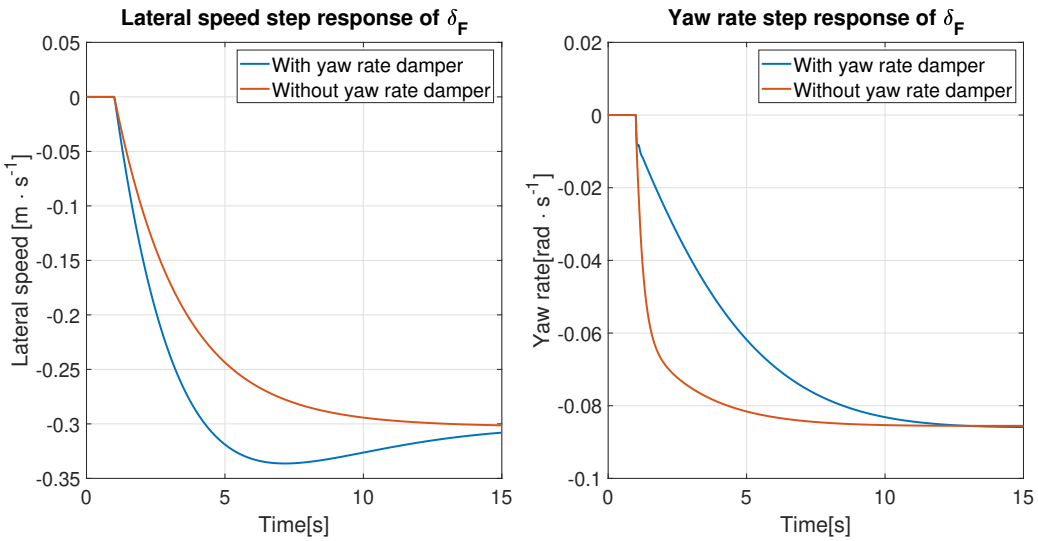

Figure 3.5. Comparison of step response between the yaw rate damper and fixed rear axle systems

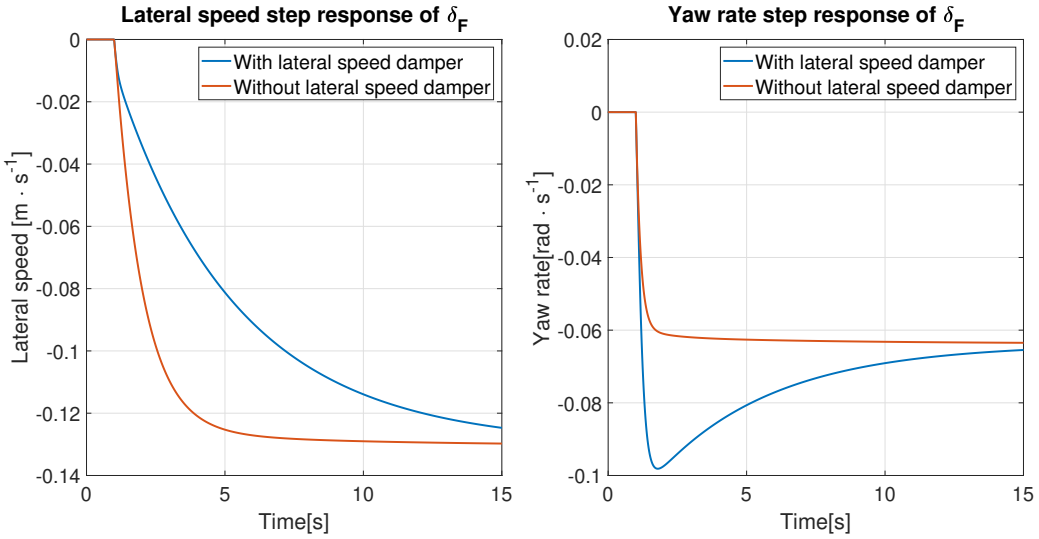

Figure 3.6. Comparison of step response between the lateral speed damper and fixed rear axle systems

3.4.3 Controllers combination

The previously described responses have shown the advantages of lateral speed damper at lower speed and the yaw rate damper at higher speed manoeuvres. The combination of both systems is implemented to create an effective rear-axle steering system at all speeds. An affine combination is used to create such system. The usage of the combination is shown in Figure 3.3. The input is the vehicle's ground speed. This value is transformed according to equation $k = \frac{v-20}{10}$ to value k. The resulting value of k is then saturated between 0 and 1. Therefore the final design uses only lateral speed damper up to $20m \cdot s^{-1}$ and yaw rate damper from $30m \cdot s^{-1}$. The values between 20 and $30m \cdot s^{-1}$ are described by the linear transition between the two controllers. The change of the overall system's response with respect to vehicle velocity is shown in Figures 3.7 and 3.8.

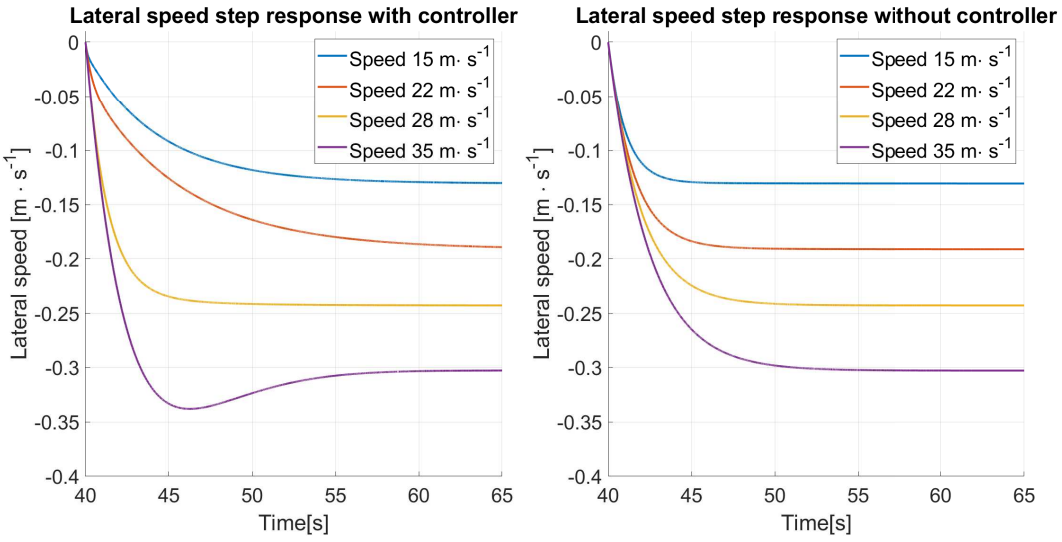

Figure 3.7. Comparison of front axle steering angle step responses between lateral speed values of a system with the controller [left] and front axle steering only design [right].

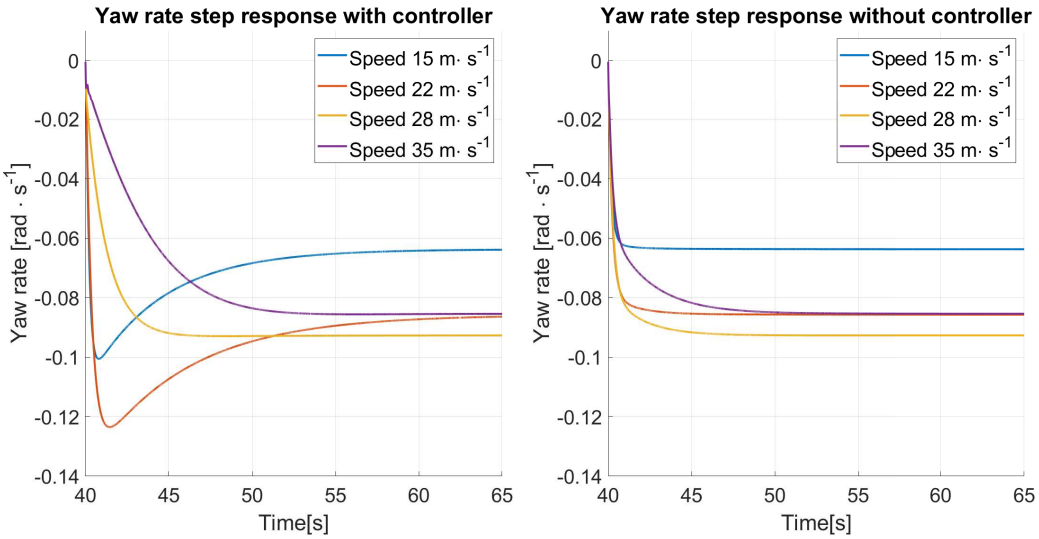

Figure 3.8. Comparison of front axle steering angle step responses between yaw rate values of a system with the controller [left] and front axle steering only design [right].

3.5 Summary

In this section, the current state-of-the-art systems, that are using rear axle steering systems, were described. As the information about these systems is limited, the feed-forward system, based on Audi four-wheel steering system, was developed. This system was created to be used as a reference for the other controllers, and it is completely dependent on the driver's input. An independent RAS system was developed to enable limited control over the vehicle states. The system still has control only over the rear wheels. Damping design was used to prevent conflicts with the driver, who is controlling the front axle. The damper controller was inspired by the aircraft industry solutions for yaw, roll and pitch damping systems.

Chapter 4
Lateral drive-by-wire system

4.1 Introduction

In the previous chapter, RAS control systems were introduced. However, these designs are not able to directly control the vehicle's states. A system with complete control over the steering angle of all four wheels should be developed to achieve the desired behaviour. For these reasons, a lateral drive-by-wire system is proposed in this chapter. This design is capable of controlling the vehicle's yaw rate and lateral speed. A complete drive-by-wire system should also be able to control the longitudinal speed. However, this feature is not developed as part of this Thesis. Instead, the driver has full control over the vehicle's powertrain.

The system has a three-level cascade control architecture, described in Figure 4.1. The inner layer controls the lateral slip angle on each wheel via the wheel's steering angle. The next layer controls the lateral speed at the PoC between each wheel and the vehicle's body by changing the requested lateral slip angle. The out-most layer directly controls the vehicle's yaw rate and lateral speed by changing the requested lateral speed at the PoC. This chapter develops control architecture for each layer independently. The robustness analysis is used to ensure the expected stability and response of the system.

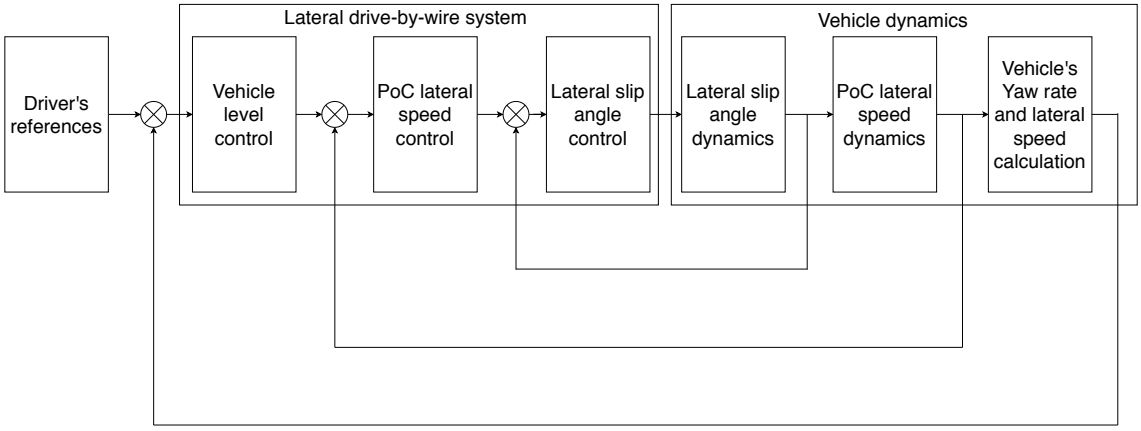

Figure 4.1. Architecture of a lateral drive-by-wire system

4.2 Lateral slip control

The wheel's lateral traction force depends on its slip angle. The relationship is shown in Equation (2.28). Therefore the vehicle states control system should include a control loop for tracking the desired slip angle. Another reason for the slip control is the non-linear dependency of the traction force on the slip angle. According to [2], each wheel has a critical slip angle, after which the tire loses traction with the ground, and the generated force is greatly reduced. By limiting the desired slip angle by this critical angle, the vehicle should not become uncontrollable. For these reasons, the slip control system is essential for dynamics shaping as well as for ensuring the vehicle stability.

4.2.1 System architecture

The lateral slip control design includes the following parts.

- Feedforward controller from α^{req} to δ
- Feedback α control loop with actuator δ
- Feedforward disturbance rejection system
- Feedback α saturation system

The overall architecture is displayed in Figure 4.2. Individual systems are described in the following text.

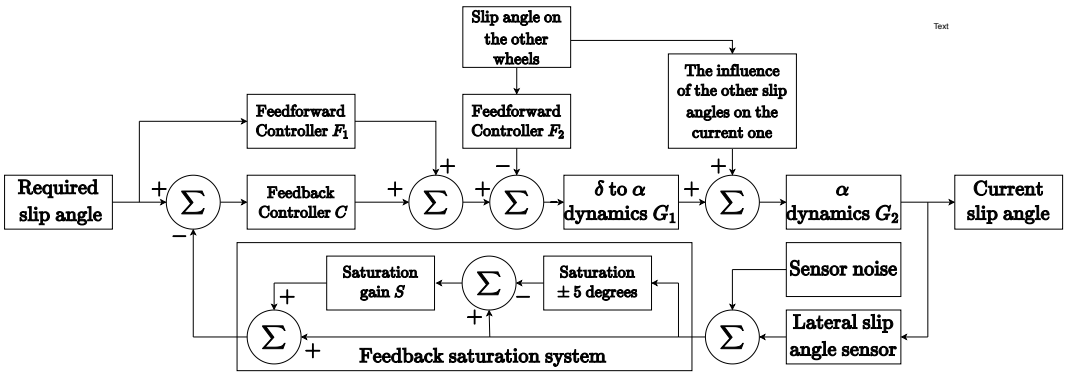

Figure 4.2. Architecture of a lateral slip control system

4.2.2 Feedforward δ to α

For the controller design, the linearized transfer function from δ to α is used. The description of this dynamics is derived in section 2.8.5. The relevant dynamics are shown in Figure 2.7. The effect of yaw rate and lateral speed on the lateral slip angle can be found by combining the Equations (2.37) , (2.38) with transformation between the vehicle states and velocities at the PoC, described in equations (2.9) to (2.16), and effect of velocities at the PoC on the α (2.40). These transformations are only multiplying the equations (2.37) , (2.38) by a constant. To use consistent description, variables G_{Yaw} and G_Y can be replaced by variables G^{α}_{Yaw} and G^{α}_{Y}. The new variables include the effect of the vehicle states on the slip angle. Overall α dynamic description can be derived from Figure 2.7 by using the calculated effect of yaw rate and lateral speed on α. The resulting relationship is described in the equation (4.2). The transfer function from δ to α without the feedback effect of vehicle states in described the section 2.8.5. The transfer function is equal to one for all driving situations (4.1).

$$G_1 = 1 \tag{4.1}$$

$$G_2 = \frac{s^2 + R_Y s}{s^2 + (R_Y - G_{YAW} - G_Y)s - G_{YAW} + R_Y} \tag{4.2}$$

The equations (4.1) and (4.2) are describing the overall transfer function $G = G_1 G_2$ with the same number of poles as zeros. Therefore, an inversion of the function exists. If the equations accurately describe the transfer dynamics, the feedforward controller in the form of the inverse transfer function of G would insure the overall dynamics from δ to α to be equal to the identity. As the real-life system is highly non-linear, such behaviour can not be expected. Nevertheless, any discrepancy will be eliminated by the feedback control loop. The designed feedforward controller uses an inversed transfer

function of the linearized system at a speed of 20 $m \cdot s^{-1}$. The system has an astatic nature and therefore can have an unexpected behaviour when crossing the saturation value for δ. An implementation of an anti-windup system prevents such behaviour. The anti-windup system uses an inversion of the controller for the back-calculation loop. Such a system has a derivation behaviour, and therefore an integrator is added in cascade with the transfer function to ensure constant response on saturation.

4.2.3 Feedforward disturbance rejection system

Each wheel's lateral slip dynamics is affected by slip angles of the other wheels. A disturbance rejection system is proposed to suppress such an effect. This system can use the linearized disturbance described in Figure 2.7. To reduce the effect of other slip angles, the calculated change of given α must be subtracted. The feedforward system turns the given wheel to decrease the disturbance effect. The transfer function from δ to α is described by equation (4.1). By combining these two relationships, overall feedforward gain can be derived. The controller changes δ by an opposite value than the calculated change of α from the disturbance.

4.2.4 Feedback control design

The previous feedforward system is unable to ensure the required behaviour for inputs at small frequencies and static signal requests. The significant problem is the lack of ability to have a zero steady-state error. This requirement is crucial. If the system is unable to ensure a zero steady-state error, it will be unable to prevent the wheel from losing traction due to the lateral slip angle higher than the calculated maximal value.

As previously mentioned, the vehicle δ to α dynamics has a derivative behaviour. Combination of this issue with the zero steady-state error requirement forces the feedback design to include two integrators. Because of the feedforward system's sufficient behaviour at higher frequencies, the feedback system can have a greatly reduced gain. The resulting design derivation has used a root-locus method. The root-locus plot is shown in Figure 4.3. The plot shows ten per-cent maximal overshoot and 0.2 seconds settling time requirements. The regulator uses two integrators and two real zeros. The gain is designed according to previously mentioned design requirements.

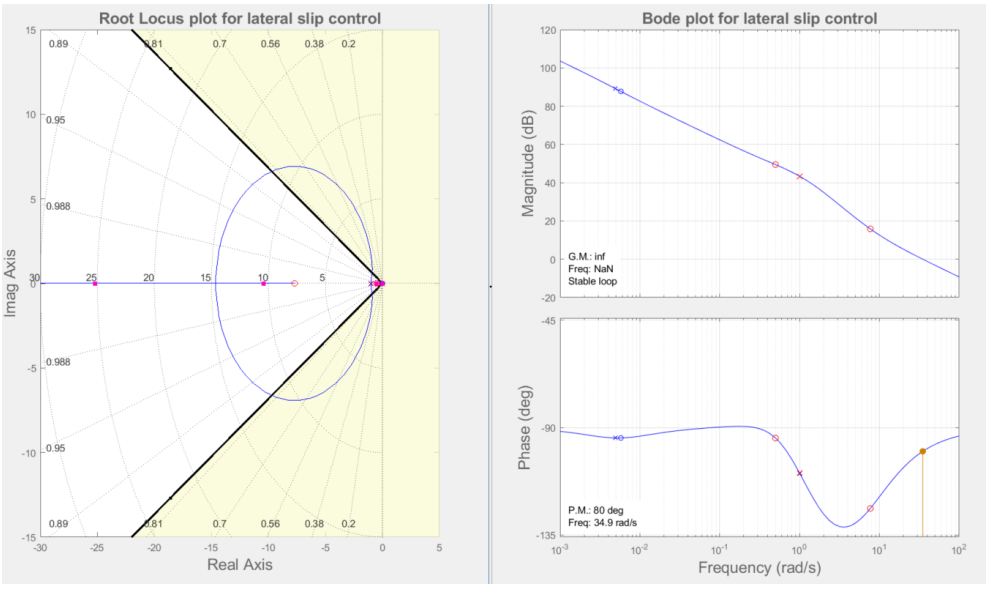

Figure 4.3. Root Locus and open-loop frequency response of the feed-back α controller

4.2.5 Robust stability and system response analysis

The resulting system behaves differently from the linearized design. The robustness analysis is necessary to verify that the closed loop behaves as expected. The robustness is tested with a considered interval of possible values for each parameter in equation (4.2). The range of values can be found by linearizing the vehicle in different scenarios. The uncertainty of the vehicle parameters, such as Pacejka parameters, should also be considered. A first-order low pass filter with a delay of 0.01 seconds is used to simulate any unknown delays in the system, like a communication lag. The resulting interval of values is used to create a set of transfer functions (4.2) with varying parameters. The robustness analysis is tested on this set.

The controller robustness stability of the feedback system should be tested first. The open-loop (OL) frequency response is used to test the closed-loop stability. The resulting response is shown in Figure 4.4.

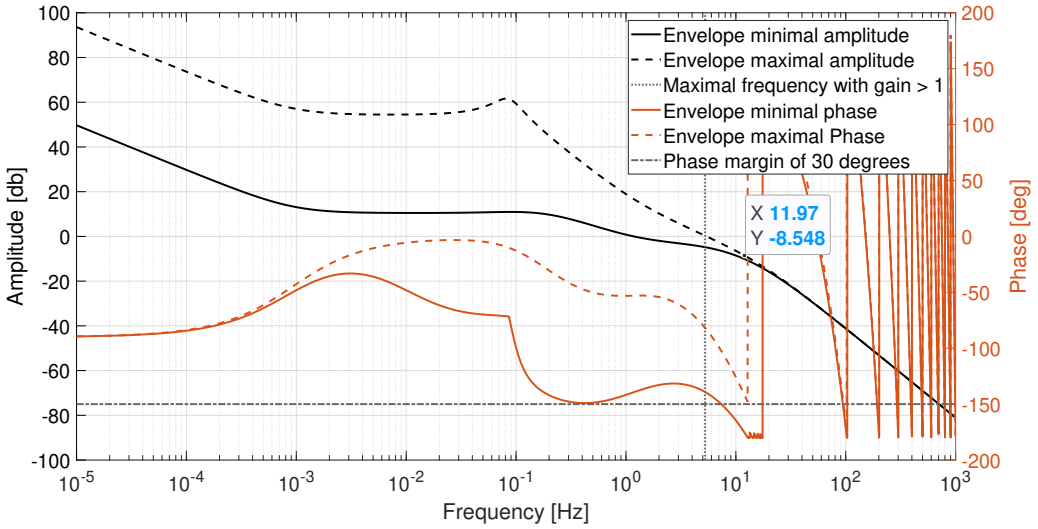

Figure 4.4. Open loop frequency response for feedback controller and model with uncertain parameters

It can be noted that the OL system has at least 30 degrees phase margin. A gain margin is at least 8 dB. The system is, therefore considered to be robustly stable.

The Basic equations of control [4, s. 210 - 215] are used to determine the robustness of behaviour. The equations are complementary sensitivity function (4.3), sensitivity function (4.4), disturbance rejection function (4.5) and noise sensitivity function (4.6). The equations are modified to reflect the designed system's architecture.

$$T = \frac{G_1 G_2 (F_1 + C)}{1 + G_1 G_2 C} \tag{4.3}$$

$$S = \frac{1}{1 + G_1 G_2 C} \tag{4.4}$$

$$PS = \frac{G_2 (D - G_1 F_2)}{1 + G_1 G_2 C} \tag{4.5}$$

$$CS = \frac{G_1 G_2 C}{1 + G_1 G_2 C} \tag{4.6}$$

The step response for each previously mentioned equation is used to show the response robustness. The result is shown in Figure 4.5. It can be noticed, that for the considered

delay and the uncertainty of parameters, the system does not have zero error in a reasonable time horizon. This problem is caused by an insufficient gain value of the controller. This value is, however, limited by the robust stability requirements and can not be increased without losing the system's robust stability. The solution uses a saturation system in the feedback loop, further described in section 4.2.6 and displayed in Figure 4.2.

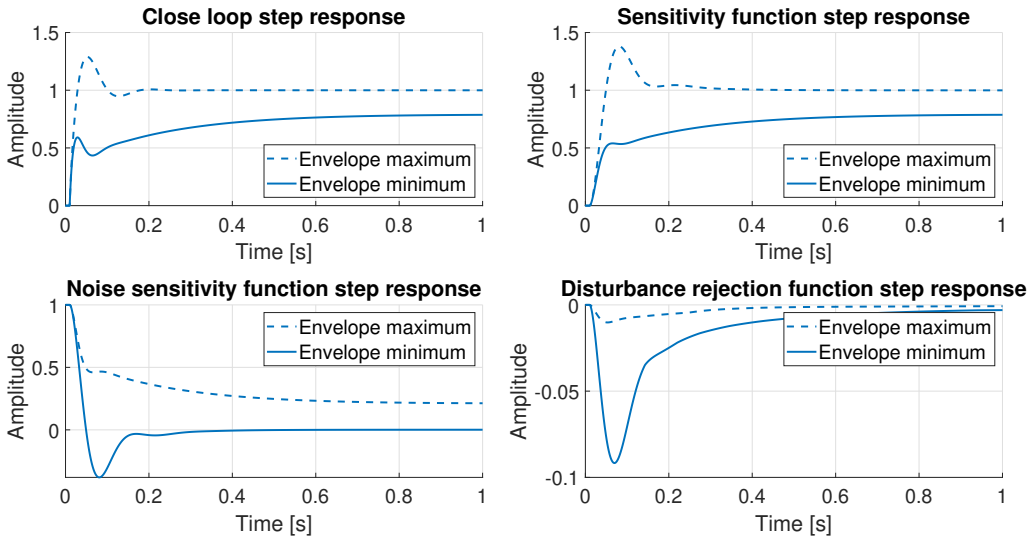

Figure 4.5. Step response of the Basic equations of control on the linearized vehicle system with varying parameters.

4.2.6 Feedback saturation system

The design of feedback saturation in the feedback loop allows the reference α to be greater than the critical angle without causing the actual α to exceed this limitation. As shown in Figure 4.5, the input-output step response achieves at least 50 per-cent of the required value in a reasonable time. The critical angle can be achieved by limiting the reference α by the double of the critical value. With a combination of these two limitations, a robust zero steady-state error can be achieved in the required time.

Method of Equivalent gain analysis [4, s. 694 - 700] is used to test the stability of the feedback saturation. Maximal gain can be found by assuming that the resulting value is not greater than the requested angle. The gain value is then 0.5. The saturation can be therefore replaced by a gain value ranging from 0 to 0.5. The limitation for saturation gain S can be found by finding the maximal feedback gain value with the stable feedback poles.

The used feedback equation is a modified version of complementary sensitivity function (4.3) with varying feedback gain C_2 (4.7).

$$T_{sat} = \frac{G_1 G_2 (F_1 + C)}{1 + G_1 G_2 C C_2} \tag{4.7}$$

The maximal gain C_2 that is robustly stable is 2.74. The saturation in Figure 4.5 is replaced by gain $\frac{SAT}{\alpha_{critical}}$. From these relationships, the following equations can be written.

$$C_2 - 1 = \frac{SAT \cdot S}{\alpha_{critical}} \tag{4.8}$$

$$\alpha_{critical} = (\alpha_{critical} - SAT) \cdot S \tag{4.9}$$

By solving these equations, the saturation value SAT is found to be 3.8789 degrees. The saturation gain S is then calculated from equation (4.8) with a value of 4.5313. This configuration is stable for all situations, included in the robust analysis. The robust analysis of this system is not included, as it can be assumed that the actual saturation system is significantly more stable than the calculated limitation. This assumption is based on the fact that the saturation behaves as gain with a maximal value of 0.5, but in most situations, the gain is significantly smaller.

4.3 Control of lateral speed on the wheels

The lateral speed at the PoC between the vehicle body and wheels directly determines the resulting car yaw rate and lateral speed. This relationship can be determined from equations (2.9) to (2.16). An advantage of controlling this velocity is the use of the lateral slip angle as the actuator of the control loop. The resulting system has then a SISO architecture. Controller architecture is shown in the Figure 4.6.

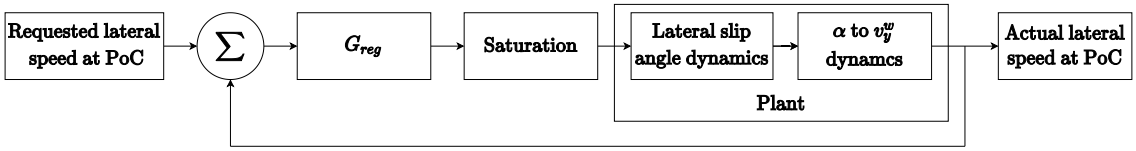

Figure 4.6. Lateral speed control architecture.

By using the α as actuator, the lateral speed dynamics at the PoC can be determined from equations for vehicle lateral speed (2.38), yaw rate (2.37) and transformation from vehicle states to v_y at the PoC (2.11) and (2.12). The resulting behaviour is described in equation (4.10), where G_Y^W and G_{YAW}^W are the DC gain values of the transfer function from α to the lateral speed at PoC through the vehicle lateral speed and yaw rate respectively.

$$tf_{v_y} = \frac{(G_Y^W \pm G_{YAW}^W)}{s} \tag{4.10}$$

A proportional regulator is used to control the dynamics. An overall transfer function is shown in the equation (4.11), where G_{reg} is the regulator gain.

$$tf_{v_y}^{reg} = \frac{G_{reg} * (G_Y^W \pm G_y aw^W)}{s + (G_r eg * (G_y aw^W + G_Y^W))} \tag{4.11}$$

The transfer function has a single pole with a time constant $\frac{1}{(G_r eg*(G_Y \pm G_y aw))}$. The resulting system has the time constant of 0.3 seconds. The output α^{req} is saturated by the double of the critical angle value. This saturation requirement was derived in the section 4.2.

4.3.1 Robust stability and system response analysis

The open-loop Bode plot is used to test the stability of the controller. The controlled system consists of α control loop and a v_y dynamics (4.10) transfer functions, connected in series. The controller is considered without non-linearities, such as the output saturation. The resulting bode plot is shown in Figure 4.7. It can be seen that the system has a significantly smaller uncertainty compared to the α control design.

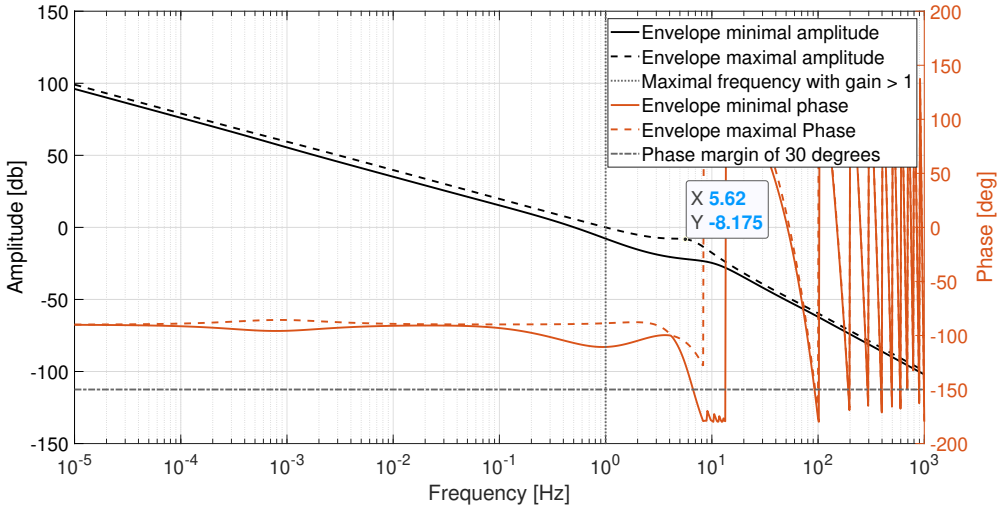

Figure 4.7. Lateral speed open loop frequency response

Four basic equations of control are used to test the robust behaviour of the controller design. The step responses for each transfer function are shown in Figure 4.8. The responses are relatively smooth and without significant problems. The only problem is the disturbance rejection response, which has sizeable steady-state gain. This is due to the integration behaviour of the lateral speed dynamics. The response is, however, not a significant issue for the system design, as the considered disturbance α should not have a constant non-zero value for a significant length of time. In the cases, when the α is constant and non zero, it can be assumed that it is saturated and therefore, the disturbance rejection system would not respond as expected.

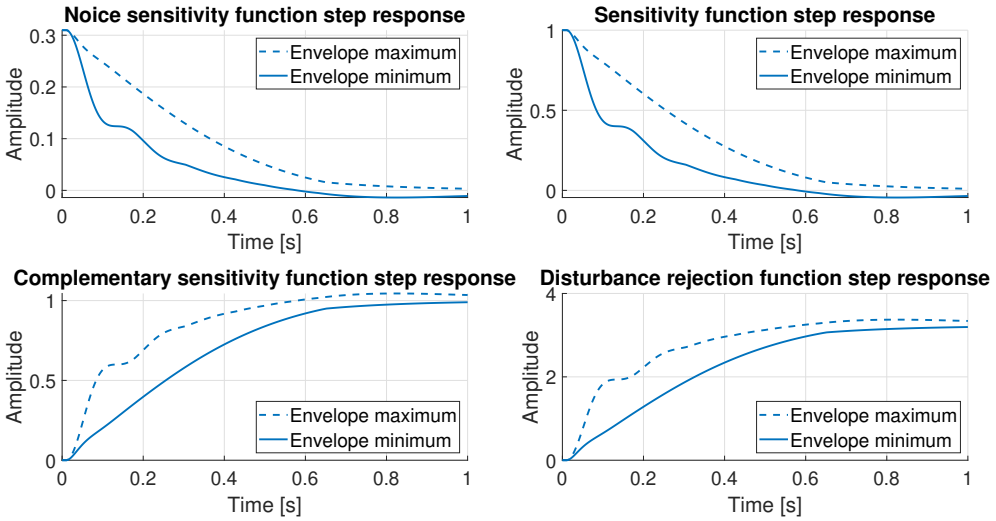

Figure 4.8. Lateral speed step response of the Basic equations of control

4.4 Vehicle level control

The last layer of the lateral drive-by-wire system is vehicle level control. The driver commands a certain yaw rate and lateral speed. The controller uses the PoC lateral speed control system, described in section 4.3 as an actuator to track these values. The

transformation of driver reference variables to the required v_y^W is described in equations (2.9) to (2.16). The resulting relationship is a linear transformation. However, simple redistribution of reference signals into v_y^W does not consider saturations of slip angles or different road conditions on each wheel. In such situations, the system might create an undesired vehicle response, as the other wheels attempt to maintain the required lateral velocity. Also, another control loop enables to shape the behaviour of the vehicle states. For these reasons, an additional vehicle level control loop was developed.

The state feedback control was used for the system design. The description of the vehicle dynamics can be derived by combining the equations (2.9) to (2.16) with the description of the PoC lateral speed control loop. This system can be described as a first-order system without zero with the time constant T, depicted in equation (4.12). For a state feedback description, both states must be measured. Therefore the C is an identity matrix and D is a zero matrix.

$$\begin{pmatrix} \dot{v}_y \\ \dot{\varphi} \end{pmatrix} = \begin{pmatrix} \frac{-1}{T} & 0 \\ 0 & \frac{-1}{T} \end{pmatrix} \begin{pmatrix} v_y \\ \varphi \end{pmatrix} + \begin{pmatrix} \frac{1}{4T} & \frac{1}{4T} & \frac{1}{4T} & \frac{1}{4T} \\ \frac{1}{4C_x fT} & \frac{1}{4C_x fT} & \frac{-1}{4C_x rT} & \frac{-1}{4C_x rT} \end{pmatrix} \begin{pmatrix} \dot{y}_{FR} \\ \dot{y}_{FL} \\ \dot{y}_{RR} \\ \dot{y}_{RL} \end{pmatrix} \quad (4.12)$$

As can be seen, the system has multiple inputs and multiple outputs (MIMO system). However, the row vectors of the matrix B are close to being perpendicular to each other. This can be confirmed by finding the dot product of the B matrix rows. If the product is equal to zero, the vectors are perpendicular to each other. The resulting value depends on the distance from each axle to the centre of gravity. For a vehicle with a centre of gravity close to the vehicle's centre, the states can be controlled independently. Therefore, the SISO state feedback control can be used.

4.4.1 State feedback control

The state feedback controller can control both the required yaw rate and lateral speed with a single design. Zero steady-state error is required to ensure the desired behaviour of the system. The error-space approach to robust tracing control design, especially Integral control with feedforward [4, s. 573 - 585], is used to achieve this requirement. The control vectors can be described according to the book example [4, s. 583]. The poles are placed as close as possible to the poles of the lateral speed at PoC loop to ensure the robust stability of the design. The Feed-forward vector does not affect the stability of the system and is therefore used to improve the system's response.

The control loop uses an integral feedback design to ensure robust tracking and disturbance rejection behaviour. The output of the state feedback control loop is the lateral speed value at the PoC for each wheel. This can cause problems as the lower-level controller is unable to track the reference signal with a too steep slope. Two approaches can be used to prevent over-integration and overshoot behaviour of the controller. The first is a static slope limitation based on the known parameters of the model. This method does not create robust behaviour in the system, as the slope differs significantly for changing external conditions such as different road surface. The second approach uses the actual and requested lateral speed to limit the maximal difference between the values. This approach is robust with respect to changing external conditions. However, it changes the behaviour of the control loop. For these reasons, the dynamic anti-windup system was implemented. The overall control loop architecture is presented in Figure 4.9. This design can be found in [4, s. 584]

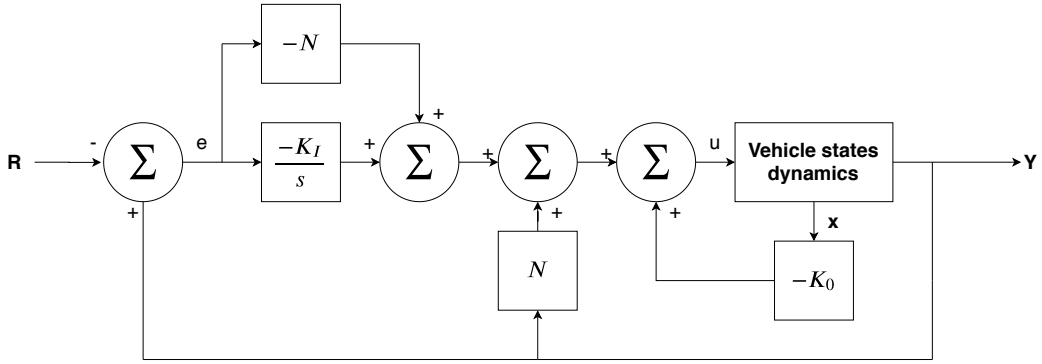

Figure 4.9. Vehicle's level control architecture

4.4.2 Robust stability and system response analysis

The open loop frequency response can be used in the same way as in the previous sections to test the robustness of the system. Each combination of inputs and outputs must be considered as the design has a MIMO architecture. The stability only dependents on the parameters of the feedback loop. The Feedforward gain vector N does not affect the stability of the system. The frequency response of the open-loop transfer function is shown in Figure 4.10. The robustness analysis of the system can be decoupled as the cross-coupling transfer functions have a maximal gain of -200 and -219 dB, respectively. Because of that, the robust behaviour analysis can be evaluated only for SISO transfer function from reference lateral speed v_y^{ref} to lateral speed v_y and yaw rate Ψ^{ref} to yaw rate Ψ. For the robust response analysis, the four Basic equations of control are used. The first transfer function, representing the overall lateral speed dynamics, is shown in Figure 4.11. The yaw rate dynamics is shown in Figure 4.12. It can be seen that the yaw rate and lateral speed dynamics are almost identical. The rise time is approximately equal to 0.2 seconds, but such behaviour is only possible for small changes of reference signals. Any larger request would saturate the α controller and therefore reduced the maximal slope of change. The overall change in behaviour should be almost not noticeable for a human driver.

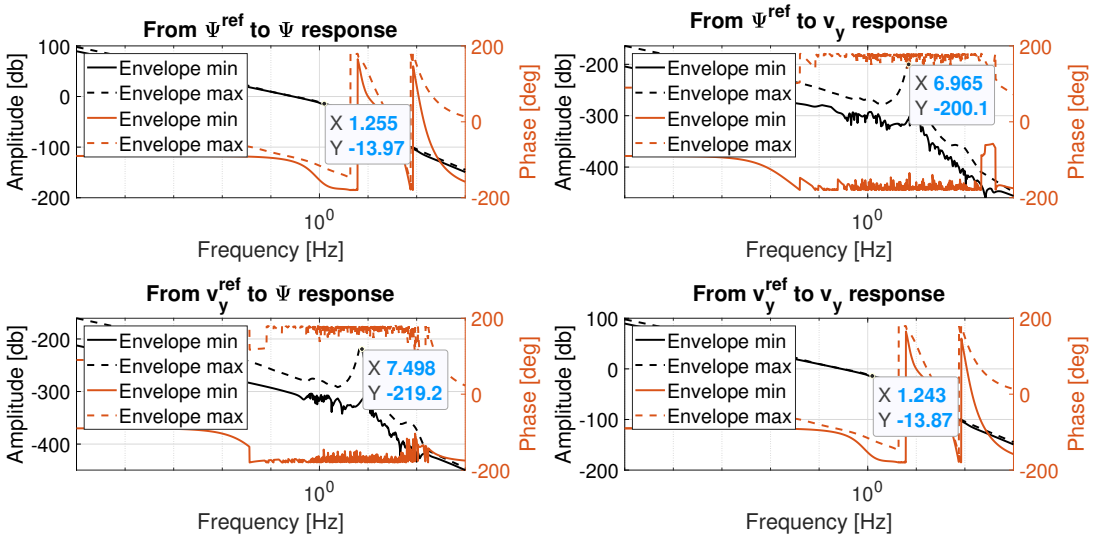

Figure 4.10. Vehicle level control open loop frequency response, where input1 and input2 are requested yaw rate and lateral speed and output1 and output2 are the resulting values of yaw rate and lateral speed

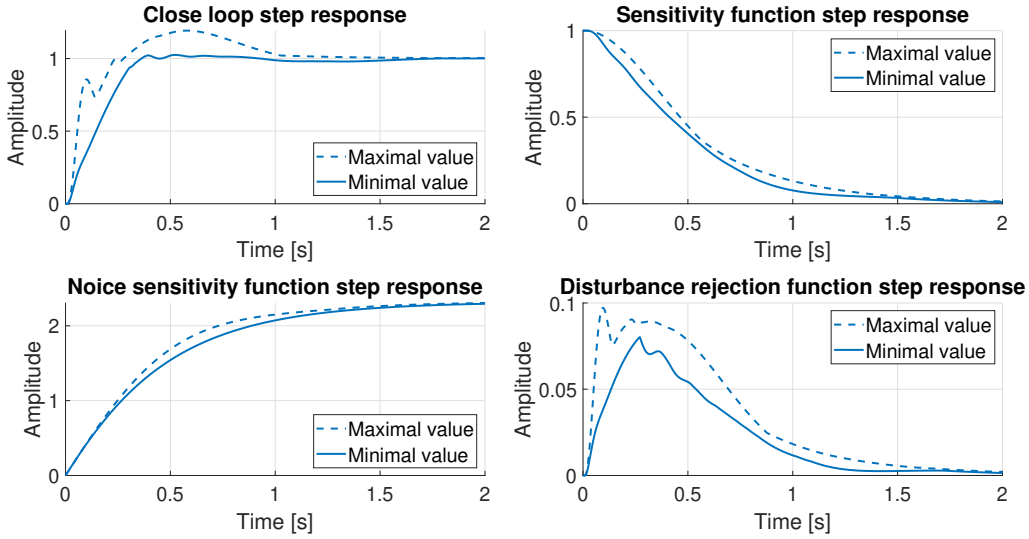

Figure 4.11. Vehicle's lateral speed response of the Basic equations of control

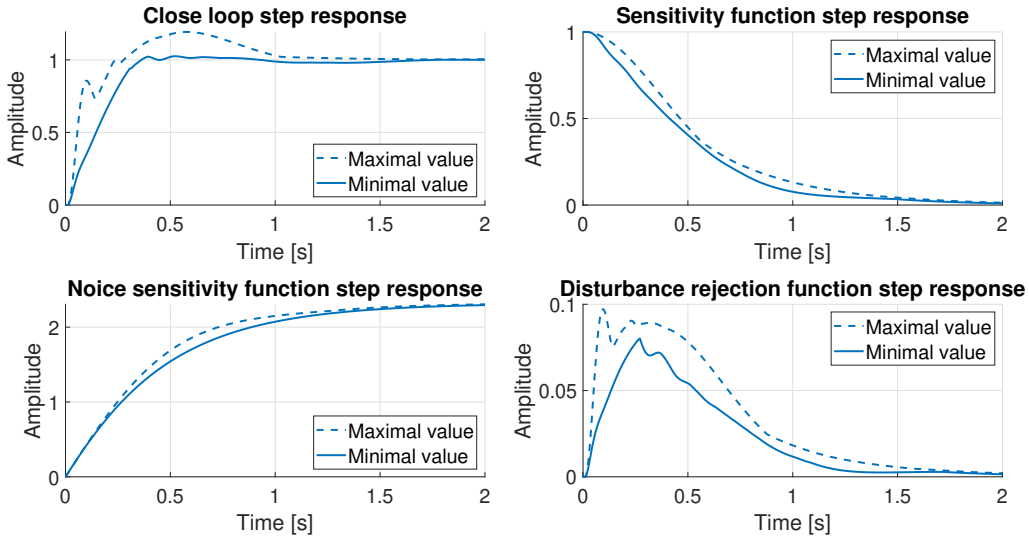

Figure 4.12. Vehicle's yaw rate response of the Basic equations of control

4.5 Summary

In this chapter, an overall drive-by-wire system was designed. The system is using four-wheel-steering to enable independent yaw rate and lateral speed control. The resulting systems robust stability and response were proven on a linearized model with varying parameters. The variance of parameters was based on the change of linearized situation and uncertainty of measured values such as Pacejka wheel parameters. Because of the three-layer controller design, the behaviour of the resulting system is sufficiently robust with respect to changing parameters and ensures stability in a wide range of conditions.

The resulting system requires either autopilot or controller with two degrees of freedom as the driver input. This opens the realm for alternative control strategies as the standard steering wheel has only a single degree of freedom. One option is a joystick controller. Another might be a modified wheel with two degrees of freedom.

Chapter 5
Verification and testing

5.1 Introduction

The vehicle model and several control algorithms were developed in the previous chapters. In this chapter, these designs will be verified on a sub-scale platform. Firstly, the mathematical model's parameters will be identified to reflect the vehicle's behaviour. Then all developed algorithms, designed with the usage of the adjusted mathematical model, will be verified and tested on the sub-scale platform.

5.2 Verification platform

The verification platform is a 1:5 car model, developed as part of Tomáš Rutrle's Bachelor's Thesis [16]. The car is an instrumented four-wheel-steering RC vehicle model with an onboard computer. The vehicle's steering angles are controlled through Matlab and Simulink programs. The platform is capable of measuring its states through onboard GPS and IMU systems. The measured variables are listed in Table 5.1.

Variable	Unit	Measuring system	Sample rate[Hz]
NED speed	$m \cdot s^{-1}$	GPS	6
Velocity Heading	deg	GPS	6
Ground speed	$m \cdot s^{-1}$	GPS	6
Acceleration	$m \cdot s^{-2}$	IMU	100
Yaw rate	$\deg \cdot s^{-1}$	IMU	100
Wheel speed	rms	Hal sensor	200

Table 5.1. Table of measured variables in verification vehicle.

The system is unfortunately not capable of measuring the body heading. Only known value is the vehicle's velocity vector heading. Due to this limitation, the platform is unable to calculate its longitudinal and lateral speed. A kinematic calculation of these states was developed as part of Tomáš Rutrle's Bachelor's Thesis [16].

This method is only accurate at low velocities and can not be used for the lateral slip control. The mathematical model is used to replace the kinematic calculation at significant velocities to solve this issue. The usage of mathematic calculation of velocities means that the calculated velocity drifts from the real value over time. For this reason, only short time experiments are used for algorithms verification.

Both vehicle velocities calculation methods are using a complementary filter to improve the accuracy of acquired platform measurements. The filter uses a combination of measured vehicle acceleration and calculated velocities to acquire the vehicle longitudinal and lateral speed of the vehicle and the velocities at the PoC, yaw rate and wheel's lateral slip ratios.

Another issue is that the current suspension setup allows a small change of the steering angle without the actuator's input. Unfortunately, the platform is unable to measure a real steering angle on the wheels. This causes uncertainty of the real steering angle and must be considered in the control system design. Also, the system is using a controller with a single degree of freedom for control input. The vehicle's engine is controlled separately from the computer. The full testing of the drive-by-wire system is, therefore, challenging.

Due to these limitations, a specific experiment must be proposed to allow for vehicle identification.

5.2.1 Vehicle identification

The mathematical model, derived in Chapter 2 is used for the platform parameters identification. The model uses two types of parameters for vehicle identification. The first describes the physical parameters of the vehicle. The second describes the traction forces generation and is based on statistical data. The physical parameters are listed in Table 5.2.

Parameter	Unit	Value
mass	kg	17.3
$C_{x,F}$	m	0.29
$C_{x,R}$	m	0.29
C_y	m	0.17
C_z	m	0.14
r_{wheel}	m	0.185
m_{wheel}	m	0.651

Table 5.2. Table of the verification vehicle's physical parameters

The traction parameters can be approximated with the usage of non-linear optimization and the following experiment. The vehicle is travelling at a constant speed with the driver repetitively turning all wheels. The front and rear wheels are turning in the same direction to minimize yaw rate and to increase the vehicle's lateral speed. The vehicle is, therefore, travelling in an almost straight line. Because of that, the platform's heading is approximately known, and the lateral velocity can be calculated.

The calculated lateral speed can be used to calculate the force, acting on the vehicle in the lateral direction. This force is assumed to be created by the traction force (2.28). For small steering angles, the generated traction force can be assumed to be parallel to the vehicle's lateral acceleration vector. Then the average force, generated by a single wheel is one-quarter of the overall lateral traction force. The average lateral slip angle is then used with the average force to compute the Pacejka parameters. The Levenberg–Marquardt non-linear optimization algorithm is used for the calculation of the values. The comparison between measured and approximated traction forces is displayed in Figure 5.1.

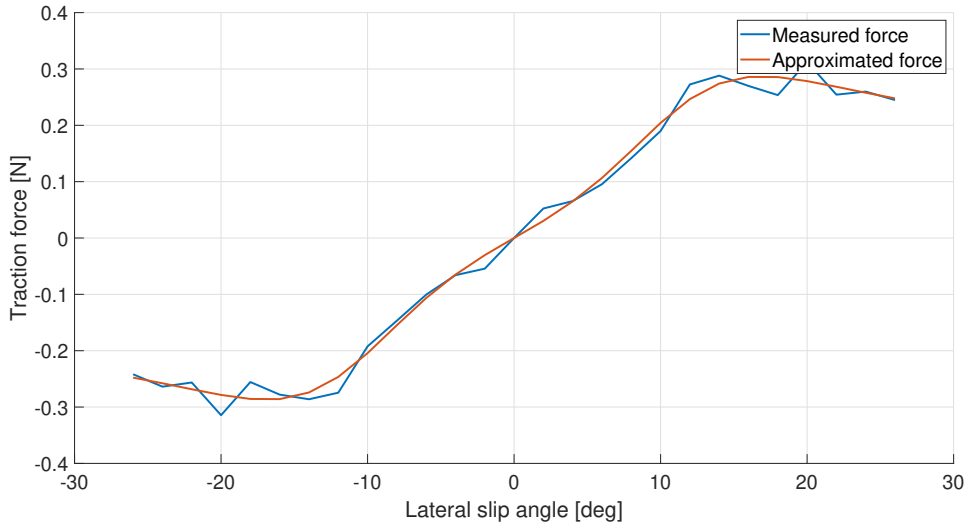

Figure 5.1. Pacejka identification.

Two sources of delay were found when comparing the measured and computed responses. The first is an approximately 0.2-second delay between the reference for steering angle and actuator's response. The second is created while calculating the lateral and longitudinal velocity. Both values are delayed by approximately 0.3 seconds. These delays significantly limit the controller's design.

5.2.2 Model verification

Several seconds of driving with changing steering angles were used to verify the mathematical model behaviour. The model received the same steering angle as the verification platform. The wheels rpm was synchronized with the measured values. The mathematical model's states are then compared with measured values to verify the model's accuracy. The comparison of vehicle states is shown in Figure 5.2. The mathematical model's response is reasonably accurate.

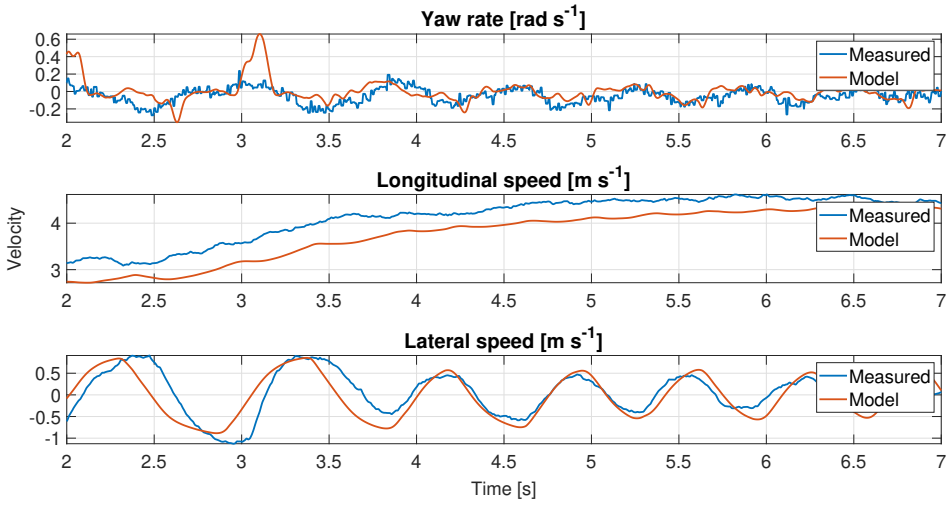

Figure 5.2. Verification of the mathematical model states behavior.

Other important values are the vehicle lateral slip angles. The comparison between measured and calculated values is shown in Figure 5.3.

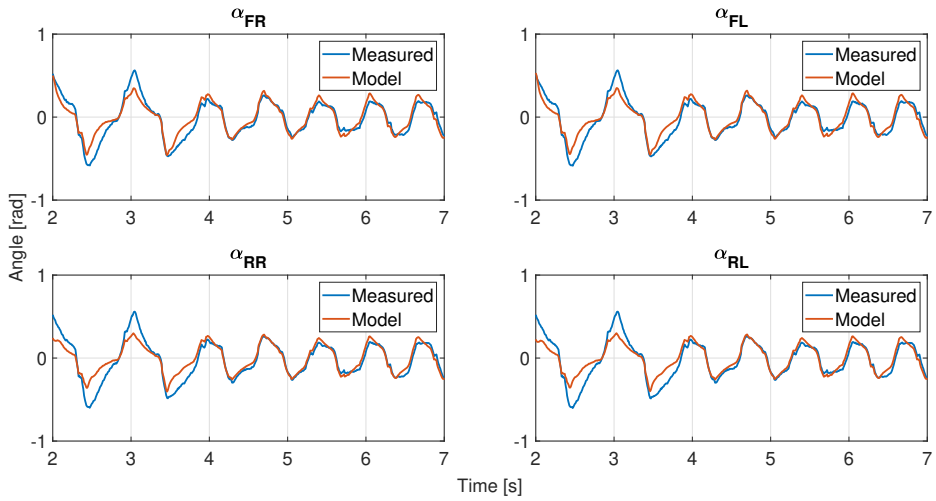

Figure 5.3. Verification of the mathematical model lateral angles behaviour.

Overall, the system's behaviour is sufficiently accurate for robust controller design. Therefore the mathematical model, derived in Chapter 2, is verified and setup according to the identified values.

5.3 Control algorithms testing

With the identified mathematical model, the control architectures derived in Chapters 3 and 4, can be implemented into the verification vehicle. The description of the control algorithms parametrization on the verification platform is not included as the design procedures are described in the previous chapters. The following text includes experiments, describing the behaviour of the verification platform, controlled by the designed algorithms.

5.3.1 FeedForward system

The feed-forward design, described in section 3.3, requires the vehicle to travel at high speeds. However, the nature of the testing situation limited the vehicle velocity to a maximum of $10m \cdot s^{-1}$. The feedforward gain had to be modified to show the behaviour of the controller. Sharp turns at varying speed were used to test the controller response. The resulting system behaviour can be seen in Figure 5.4.

The system turns the rear wheels in the opposite way than the front wheel steering in velocities, higher than $4m \cdot s^{-1}$. The positive gain significantly increases the lateral vehicle speed. This behaviour is noticeable at time 50 to 60 seconds in the experiment. The lateral slip angle on the wheels reaches up to fifty degrees in lower speeds. The higher slip angle corresponds to the counter-steering situations. On the other hand, the positive gain seems to decrease the slip angles at higher speeds significantly. From this observation, we can assume that the positive gain increases vehicle stability, as the range of steering angles that does not result into the loss of traction is widen, while the negative gain decreases it. This conclusion confirms the expected behavior, described in section 3.3.

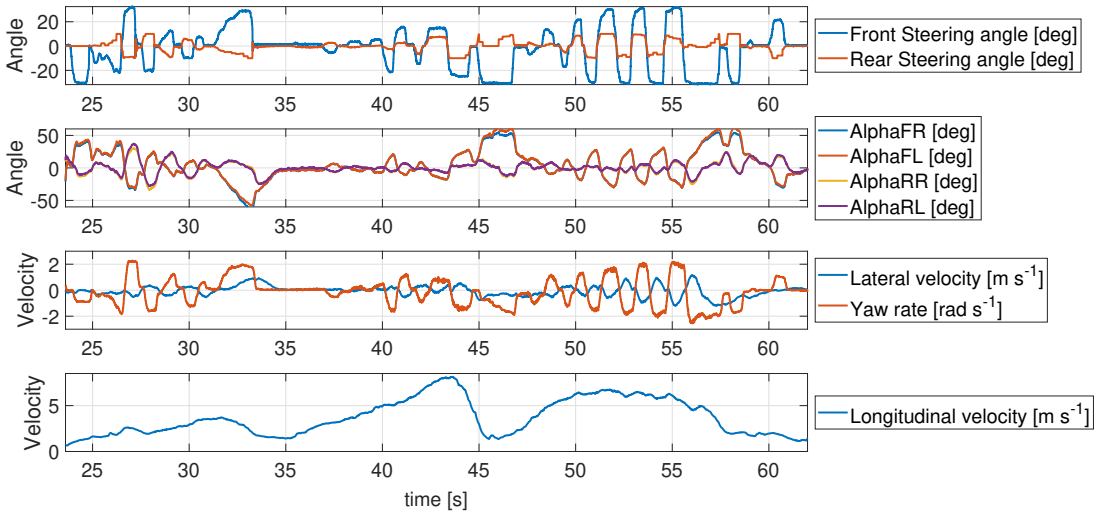

Figure 5.4. Response of feed-forward control, implemented on the verification platform.

5.3.2 Independent rear axle steering control

The vehicle states damper, proposed in section 3.4 is implemented on the verification platform and set up in a way to demonstrate the system's behaviour. Because the system architecture allows significant change of the damper gain, the controller was set without the usage of the mathematical model. Only yaw rate damper was used due to the considerable delay in lateral speed calculation. The delay made the system difficult to control. The yaw rate damper response is shown in Figure 5.5. The response demonstrates the damping effect of yaw rate's high frequencies. The rear axle steering angle reacts on step change of front steering angles with a delay of approximately 0.2 seconds. After the initial reaction, the rear axle returns to zero turn angle due to washout filter. The resulting system tries to resist sharp changes of the yaw rate but does not affect constant values such as long turns. A long turn can be seen at the last two seconds of the experiment, there the yaw rate is nearly constant.

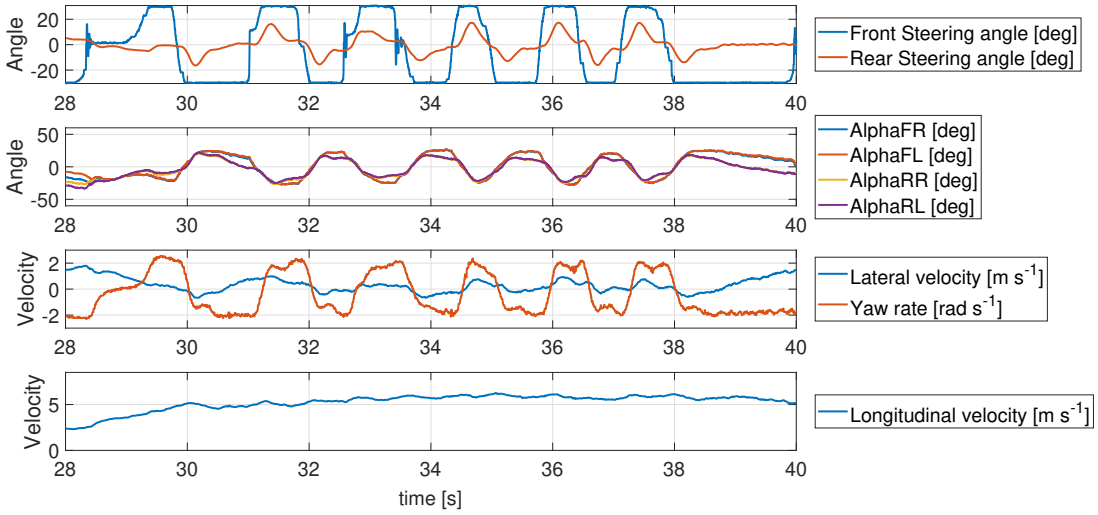

Figure 5.5. Response of yaw rate damper, implemented on the verification platform.

5.3.3 Lateral slip angle control

The first part of the implementation of the drive-by-wire system on verification platform is the design of lateral slip control loop according to the approach, described in section 4.2. Due to limitations in the vehicle design, the control architecture was reduced by the feed-forward disturbance rejection control. During experiments, the control system is only active at speeds grater than $4m \cdot s^{-1}$. In lower speeds, the driver directly controls the front axle while the rear axle is fixed to zero. The command to α at low speed is zero. Two different situations are used to show the behaviour of the resulting system. The first is control with the same α request for the front and the rear axle, displayed in Figure 5.6. The second is the situation with the opposite request for front and rear axle, shown in Figure 5.7. The resulting system is capable to track the requested lateral slip angle in both situations. However, the system has difficulties to follow fast changing requests. Overall it is clear that the delay, caused by the steering system, significantly reduces the designed lateral slip control capabilities.

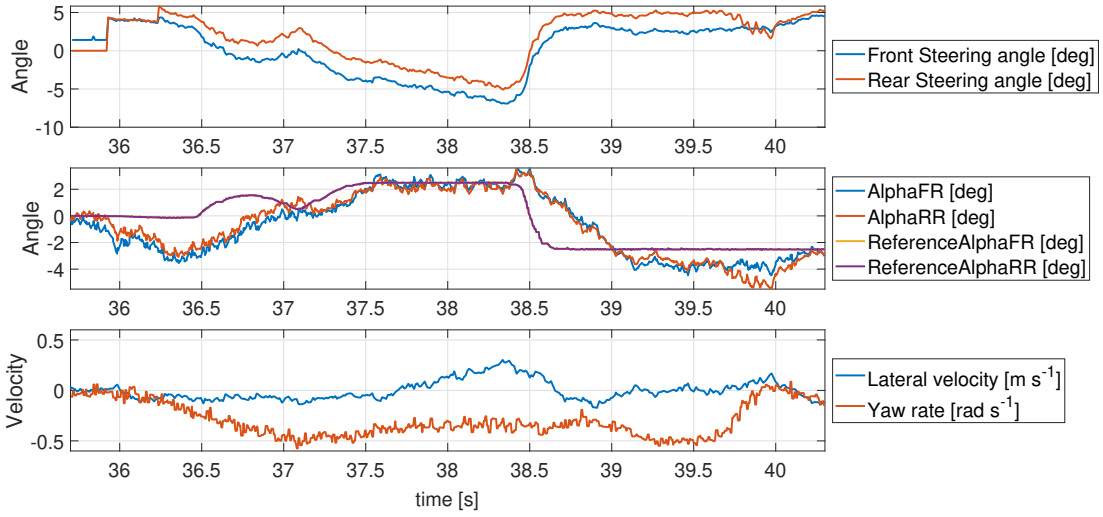

Figure 5.6. Response of alpha control loop with the same request for front and rear axle.

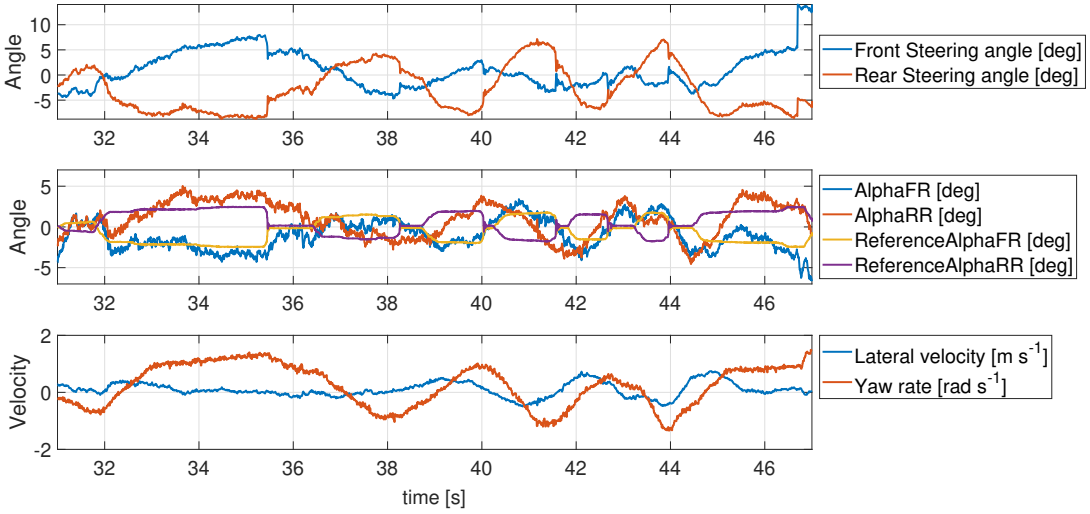

Figure 5.7. Response of alpha control loop with an opposite request for front and rear axle.

The most important feature of lateral slip control is the capability to keep the vehicle controllable by limiting the lateral slip angle. This behaviour is greatly improved with the usage of the feedback saturation system. This system creates significantly smaller slip overshoot over the critical angle. During the experiment, the critical angle was set to 10 degrees. The driver requests lateral slip angle with values ± 10 degrees. The system response without feedback saturation is shown in Figure 5.8 while the system with saturation is shown in Figure 5.9. In both situations, the request for α changes in the order of seconds. The system without saturation has up to fifty per-cent overshot, while the system with saturation has minimal or no overshoot. As the saturation system does not affect smaller angles, the responses in Figures 5.6 and 5.7 have noticeable overshoot even with implemented saturation.

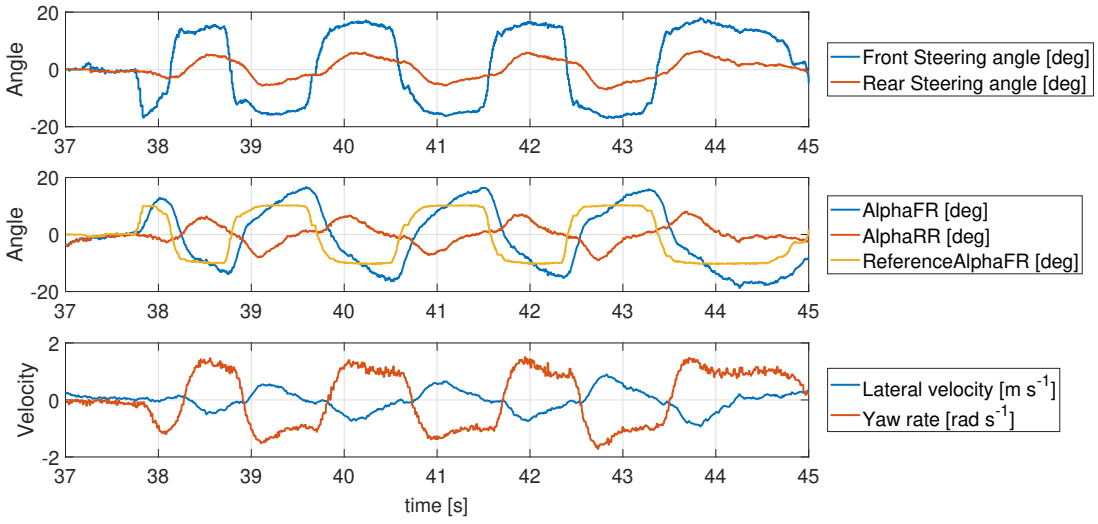

Figure 5.8. Response of alpha control loop on front lateral slip angle request.

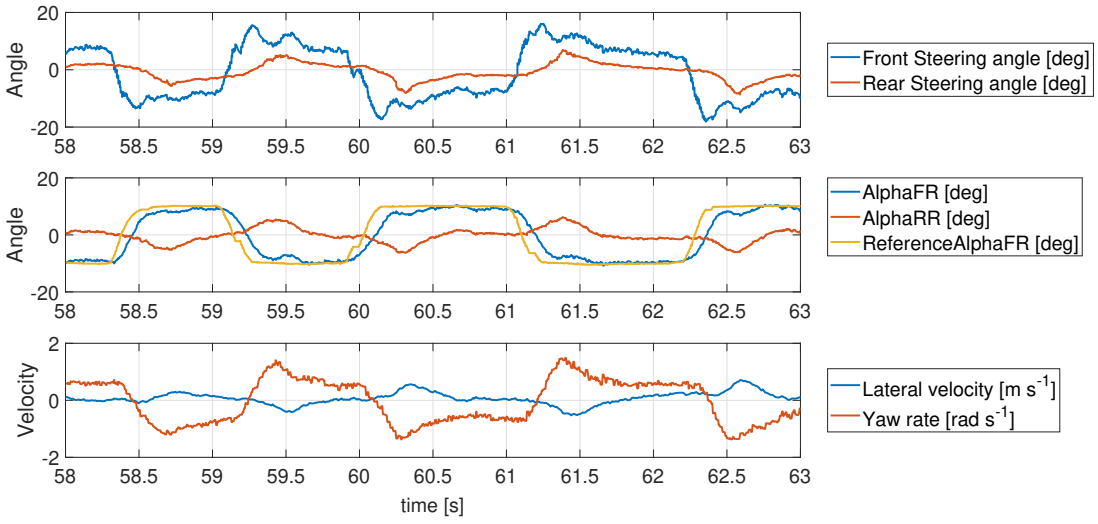

Figure 5.9. Response of alpha control loop with feedback saturation on front lateral slip angle request.

5.3.4 Lateral drive-by-wire system

After verification of slip control, a complete lateral drive-by-wire system is tested. This design includes three control loops. Each loop's response is presented, and the resulting behaviour is described. The drive-by-wire system has two degrees of freedom, but the verification vehicle uses a controller with only one degree of freedom. For this reason, several experiments were conducted. The first experiment is yaw rate tracking while requesting zero vehicle's lateral speed. The resulting response of yaw rate and lateral speed is shown in Figure 5.10. The lateral speed at the PoC is presented in Figure 5.11 and lateral slip angle in Figure 5.12.

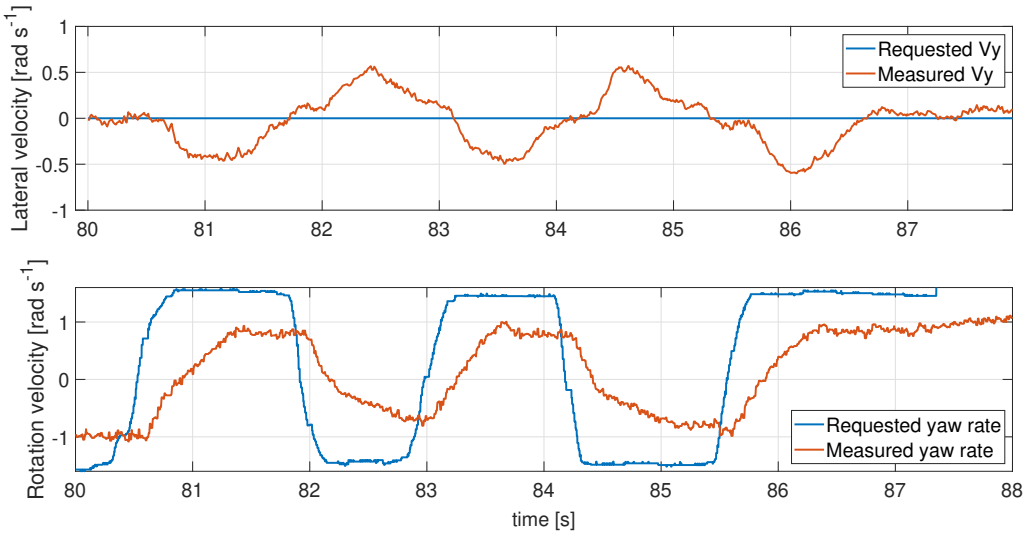

Figure 5.10. Yaw rate response of drive-by-wire system.

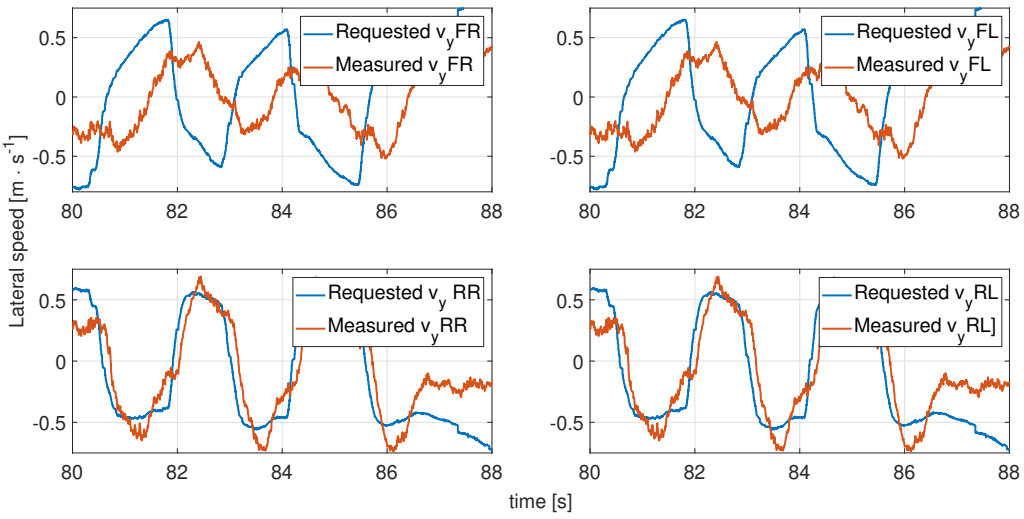

Figure 5.11. Lateral speed at PoC response of drive-by-wire system.

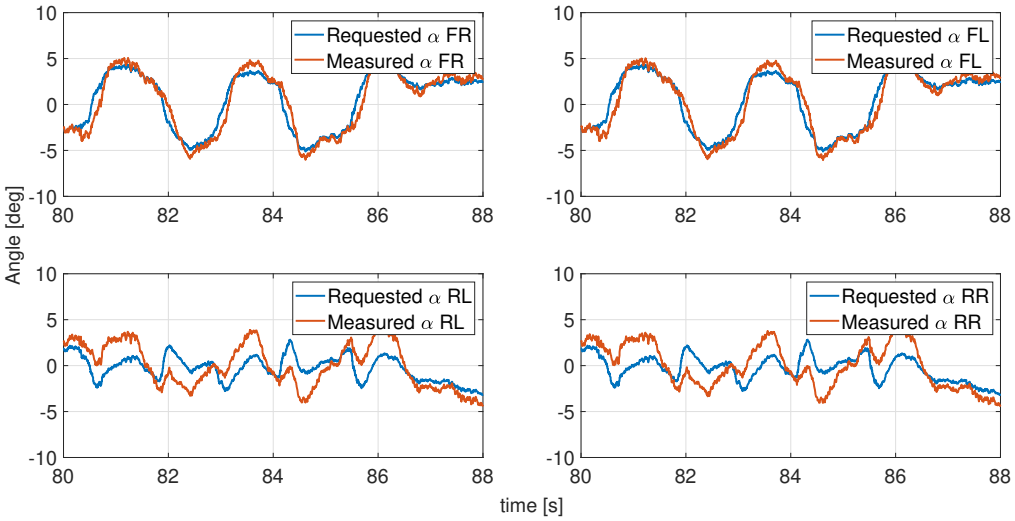

Figure 5.12. Lateral slip angle response of drive-by-wire system.

The resulting system is capable of tracking the requested yaw rate. However, the response has a large steady-state error and rise time. The steady-state error could be reduced by accurately set the feed-forward part of state control. Such a solution is, however, not robust. The system is capable of reducing the lateral speed of the vehicle but is not capable of keeping zero value during the experiment. Combination of yaw rate and lateral speed request is used to show the capability of the system to track two states simultaneously. The controller responses are shown in Figures 5.13, 5.14 and 5.15. The system is capable of tracking requested yaw rate and lateral speed. However, the lateral speed seems to be unable to keep a constant steady-state error. This issue seems to be created by an insufficient gain in lateral speed and PoC control system. This gain is, however, limited by the robust stability requirements. This means that the design is unable to control both lateral speed and yaw rate on the verification vehicle. The solution can be either redesign of verification vehicle or the control system.

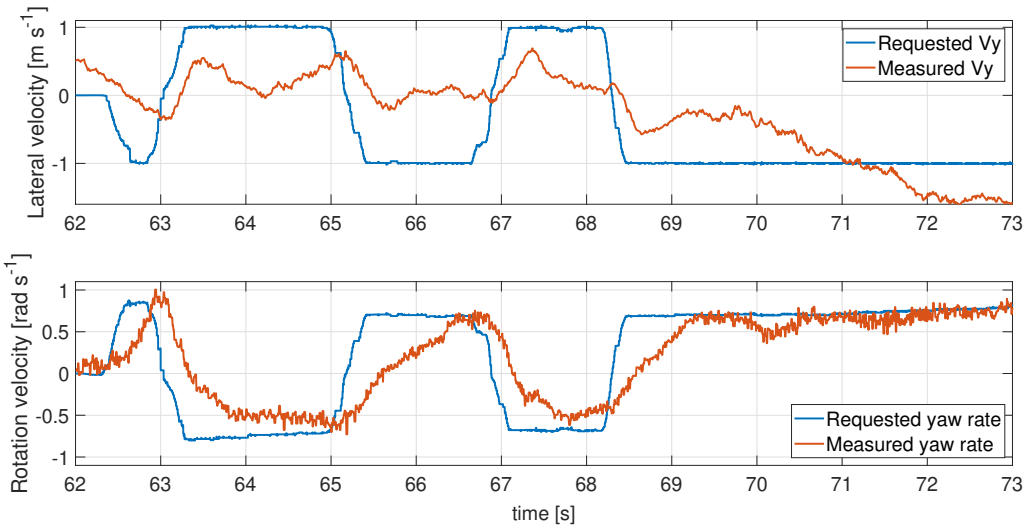

Figure 5.13. Yaw rate response of drive-by-wire system.

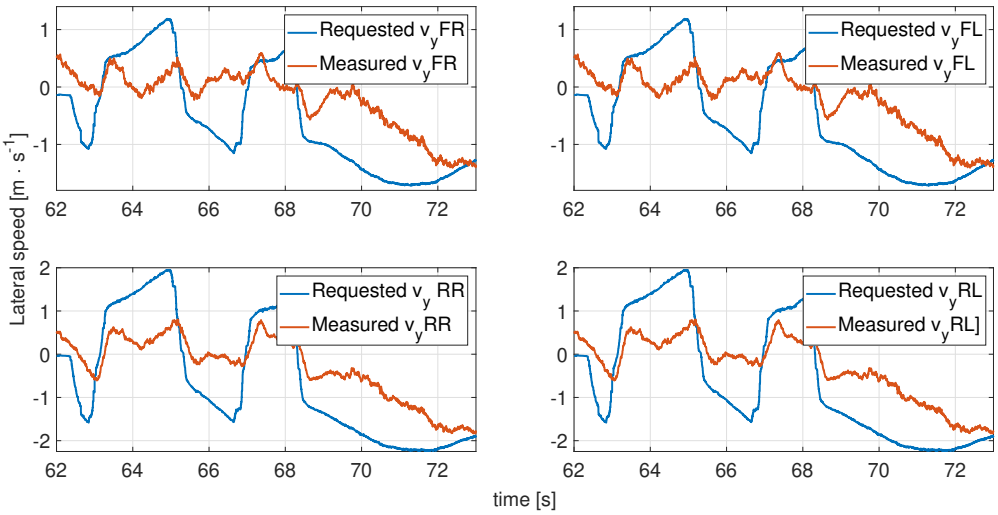

Figure 5.14. Lateral speed at PoC response of drive-by-wire system.

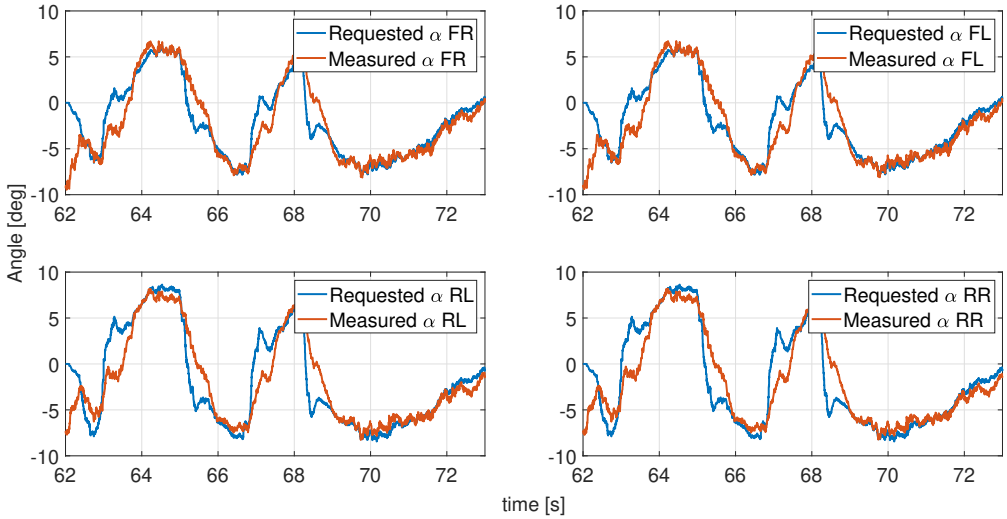

Figure 5.15. Lateral slip angle response of drive-by-wire system.

5.4 Summary

The verification of developed algorithms was done in this Chapter. Firstly, the vehicle mathematical model was set to fit the verification platform dynamics. This model has then been used to set up the developed algorithms on the verification platform. Secondly, the controllers were implemented and tested on the vehicle. The resulting vehicle responses were presented and debated. The lateral drive-by-wire system testing had to be divided into only yaw rate and a fixed combination of yaw rate and lateral speed control due to the platform's control interface with a single degree of freedom. Each design was successfully tested and debated in depth. The biggest problem for the control systems was found to be the inaccurate lateral speed measurement. The problem limited the drive-by-wire system's ability to control the vehicle states simultaneously. This issue needs to be fixed to enable any future development.

Chapter 6
Results

The work successfully achieved all the initial goals, proposed in section 1.2. A quick overview of the results is listed below.

- Linear and non-linear twin-track mathematical model was derived in Chapter 2. This model was developed with rapid algorithms development and simple vehicle identification in mind.
- The review of existing academia/industry solutions can be found as part of Chapter 3. The most promising system seems to be Audi and Porsche's rear-axle steering. Due to limited information, a control system, based on Audi's design, was developed to show the potential of rear-axle steering.
- To increase the influence of RAS system, an independent RAS control was developed in section 3.4. This system dampens the vehicle's yaw rate or lateral speed to increase the car's agility in lower and stability at higher speeds.
- The lateral drive-by-wire system, operating all the vehicle's steering angles was developed in Chapter 4. The system uses wheels lateral slip control to ensure robust behaviour and stability of the system. Resulting design enables direct control of the vehicle's yaw rate and lateral speed.
- All the proposed systems were successfully verified and tested on a 1 to 5 scale vehicle verification platform in Chapter 5. The drive-by-wire testing was reduced to only yaw rate control or fixed combination of lateral speed and yaw rate control due to the problems with the vehicle's lateral velocity estimation and the control interface's insufficient degrees of freedom. For the complete system verification, significantly more accurate acquisition of lateral speed needs to be developed.

6.1 Future Work

The sub-scale platform's measurement limitations had a significant effect on the verification process. For future development, the platform should be modified according to the following points.

- Inclusion of a GPS position measurement, capable of measuring the vehicle body heading
- Reduction of the time delay, present in the steering system
- Inclusion of a wheels steering angle measurement system
- Creation of a sophisticated sensor fusion algorithms to ensure accurate measurement of lateral and longitudinal velocities at least at 100 Hz

With a modified verification platform, more sophisticated testing can be concluded. The future development phase should include tests, that show not only the behaviour of the system but also the improvements over the traditional front axle steering architectures.

Chapter 7
Conclusion

The lateral dynamics control strategies of independent four-wheel-steered vehicles were developed in this thesis. The current industry 4WS systems are using only rear axle control, based on the front axle steering angle and vehicle's speed, where the front axle is still under the driver's control. Such systems modify the car's behaviour to make it more agile at low speed and more stable at high speed. However, it is far from fully exploiting the possibilities of full Drive-by-wire system.

After reviewing the current industry solutions of 4WS, it is clear that only independent control of all four wheels can provide the desired vehicle's behaviour and stability. Such design then acts as a vehicle level control system and reshapes the car's dynamics into a relatively simple to use system for the human operator. This property significantly increases the vehicle capabilities from the driver's point of view. The implementation of such a design can significantly reduce computing power requirements for any autopilot systems as the drive-by-wire system solves any issues arising from complex and non-linear vehicle dynamics, including challenging handling of the tire to road interface.

This thesis proposed the lateral drive-by-wire system, capable of steering all four wheels to control the vehicle's yaw rate and lateral speed. The design method included the derivation of the mathematical description of a twin-track vehicle, design of controller with the usage of SISO LTI control laws and the successful verification of the algorithm of the sub-scaled platform.

One significant problem accoutered was inaccurate lateral speed measurement due to lack of body heading measurement capabilities. This issue limited drive-by-wire testing. Although the regulation of yaw rate worked as expected, the combined control of yaw rate and lateral speed proved to be unreliable. However, the system was successfully tested in simulations. As the yaw rate control testing confirmed the simulated behaviour, it can be assumed that the controller with accurate lateral speed measurement would be able to regulate both vehicle states simultaneously.

Appendix A
Acronyms

CoG	Center of gravity
GPS	Global position system
IMU	Inertial measurement unit
LTI	Linear-time-invariant
NED	North east down
PoC	Point of contact
RAS	Rear axle steering
RC	Remote control
SISO	Single input-Single output
4WSC	Four wheel steering control

References

[1] Dieter Schramm, Manfred Hiller, Roberto Bardini. Vehicle Dynamics. Duisburg 2014.

[2] Hans B. Pacejka. Tire and Vehicle Dynamics. The Netherlands 2012.

[3] Dean C. Karnopp, Donald L. Margolis, Ronald C.Rosenberg. SystemDynamics. Hoboken, N.J. 2013.

[4] Franklin, Powell, Emami-Naeini. Feedback Control of Dynamics Systems. Prentice Hall, USA 2019.

[5] Robert Bosch GmbH. Bosch automotive handbook Plochingen, Germany

[6] Raymond Brach and Matthew Brach. The Tire-Force Ellipse (Friction Ellipse) and Tire Characteristics SAE International 04/12/2011.

[7] Moad Kissai, Bruno Monsuez, Adriana Tapus, Didier Martinez. A new linear tire model with varying parameters. 2017 2nd IEEE International Conference on Intelligent Transportation Engineering (ICITE), Sep 2017, Singapore, Singapore.

[8] R.E. Colyer FIEE and J.T. Economou AMIEE,S'MIEEE . Comparison of Steering Geometries for Multi-Wheeled Vehicles by Modelling and Simulation Department of Aerospace, Power and Sensors, CRANFIELD University-RMCS,Shrivenham, Swindon 1998

[9] Leonardo Marín, Marina Valles, Ángel Soriano, Ángel Valera and Pedro Albertos. Event-Based Localization in Ackermann Steering Limited Resource Mobile Robots

[10] Protean . Homepage - Protean. [online] Available at: www.proteanelectric.com [Accessed 5 May 2020].

[11] Mercedes-benz. 2020. VISION AVTR. [online] Available at: www.mercedes-benz.com/en/vehicles/passenger-cars/mercedes-benz-concept-cars/vision-avtr [Accessed 5 May 2020].

[12] Audi Technology Portal Audi Q7 all-wheel steering [online] Available at: www.audi-technology-portal.de/en/chassis/wheel-suspension-steering/audi-q7-all-wheel-steering-eng [Accessed 5 May 2020].

[13] Porche Rear-axle steering [online] Available at: www.porsche.com/international/models/911/911-gt3-models/911-gt3/drive-chassis/rear-axle-steering [Accessed 5 May 2020].

[14] Munther A. Hassouneh, Hsien-Chiam Lee and Eyad H. Abed. Washout Filters in Feedback Control: Benefits, Limitations and Extensions. American Control Conference Boston, Massachusetts June 30. July 2,2004

[15] Pascal Traverse, Isabelle Lacaze and Jean Souyris. AIRBUS FLY-BY-WIRE: A TOTAL APPROACH TO DEPENDABILITY Airbus, 316, route de Bayonne, 31060 Toulouse, France

[16] Tomáš Rutrle. Bachelor's Thesis: Development of verification platform for over-actuated vehicles CTU Prague 2020